Impact of large-scale climate variability on the Arabian Sea coastal upwelling system

Dissertation

zur Erlangung des Doktorgrades
an der Fakultät für Mathematik, Informatik und Naturwissenschaften
im Fachbereich Geowissenschaften
der Universität Hamburg

vorgelegt von

Xing Yi

Hamburg 2016

Tag der Disputation:

26.01.2017

Gutachter:

Dr. Eduardo Zorita

Prof. Dr. Kay-Christian Emeis

Abstract

Coastal upwelling advects nutrient-rich water masses from deeper layers to the surface layers, supporting areas of high ocean biological productivity. It is thus important to characterize the variations of upwelling intensity caused by natural drivers and by global climate change. In general terms, coastal upwelling is primarily caused by Ekman pumping driven by along-shore wind-stress. Upwelling variability may be caused by variations in the wind strength but also by other factors modulation of the water column stability, like thermal stratification.

The western coast of the Arabian Sea, together with other four major upwelling systems located in the Eastern Boundaries of the major mid-latitude oceans, is one of the most important upwelling systems in the world. In this thesis, I statistically analysed various data sets, including simulations with ocean-only and coupled atmosphere-ocean models, together with observations and meteorological reanalysis data with the aim to examine the variation of the Arabian Sea upwelling and the mechanisms that are responsible for it during last centuries and the 21st century. The use of model simulations is required due to the difficulty of monitoring variations in ocean vertical velocities over long periods of several decades and longer. Upwelling intensity is represented by the models by simulated vertical velocity, which is considered to describe the upwelling more directly than the upwelling proxies derived from other variables. The study is divided into three parts based on the focusing time periods: the present (1950-2010), the past (850-1849), and the future (2006-2100).

A very high resolution (10 km) global ocean simulation was analysed to study the Arabian Sea upwelling over the last 61 years, with an ocean-only simulation driven by meteorological observations. The modelled vertical velocity reveals an annual cycle indicating that the upwelling starts in May and ends in September. In terms of long-term variability, the upwelling does not show any significant trend over the modelled period. The upwelling has strong correlations with the sea surface temperature and the along-shore winds. Contrary to current expectations, the correlations between the upwelling and the Indian Monsoon indices are rather low, which implies that processes other than the Indian Monsoon might have an impact on the upwelling. I could identify a pattern of climate variability different from the one that drives the Monsoon and that more clearly contributes to drive the upwelling variability. Moreover, although the upwelling and the Monsoon are linked to similar near-surface temperature patterns in South Asia, the mechanisms behind these links are different.

I also examined the Arabian Sea upwelling over the last millennium as simulated by two Earth System Models. An ensemble of three simulations with same external forcings but different initial conditions is used, allowing separating the influence of external forcing and internal variability. In general, the two models present quite similar results. In contrast with the results obtained in the first part of the thesis, the simulated upwelling here has significant correlations with the Indian Monsoon. The simulated evolution of upwelling also agrees with that derived from sediment records. A consistent negative long-term trend of the upwelling is revealed in all simulations over this period, suggesting that influence of common external forcing acts at this long time-scale. The analysis of the sea level pressure patterns in these simulations reveals similarities with simulations of the mid-Holocene and thus indicates that the upwelling trends are caused by the orbital forcing.

The last part of the thesis focuses on the future warming scenarios simulated by essentially the same Earth System Models used in the last millennium analysis. These simulations indicate future reduction of upwelling intensity in the RCP8.5 scenario, the one with strongest future emissions, which is at first sight in contrast to the strengthening of the upwelling favourable along-shore

wind simulated in this scenario. The analysis in the vertical profiles of the upwelling and the sea temperature leads to the conclusion that the weakening of upwelling in the RCP8.5 scenario is caused by the stratification of the surface water due to the strong warming effect. Scenarios with a weaker increase of greenhouse gases in the atmosphere, like the RCP2.6 scenario, show no significant trend in the upwelling or the wind. These simulations thus show that the causes for upwelling trends in the future may be different from the factors affecting present and past upwelling variability.

One important caveat affects the conclusions derived from this thesis. Coastal upwelling is a process that occurs at small spatial scales, and present computing capabilities prevent long simulations with very high-resolution models. Therefore, these conclusions should be ascertained in the future when these simulations with coupled high-resolution models can be carried out.

Zusammenfassung

Küstennahes Upwelling (Auftrieb) bringt nährstoffreiche Wassermassen aus der Tiefe in die oberflächennahen Schichten und sorgt dadurch für eine hohe biologische Produktivität in diesen Ozeanregionen. Es ist daher wichtig die Variabilitäten des Auftriebs, verursacht durch natürliche Faktoren und durch den globalen Klimawandel, zu identifizieren. Ekman Pumping ist der Hauptantrieb für küstennahes Upwelling, welches wiederum durch den küstenparallelen Windstress hervorgerufen wird. Variabilitäten in der Stärke des Windstresses können somit zu Variationen im Upwelling führen. Aber auch andere Faktoren wie die Stabilität der Wassersäule durch thermische Schichtung können die Intensität des Upwellings beeinflussen.

An der Westküste des Arabischen Meeres befindet sich eines der fünf großen Küstenauftriebsregionen der Welt. Zu denen zählen außerdem die vier Ostrandstromauftriebsgebiete in den Subtropen des Pazifiks und Atlantiks. In meiner Doktorarbeit habe ich anhand verschiedener Datensätze (Ozeansimulationen, gekoppelte Atmosphäre-Ozean Simulationen, Beobachtungsdaten und meteorologische Reanalysen) die Variationen des Upwellings im Arabischen Meer und die dafür verantwortlichen Antriebe während der letzten Jahrhunderte und dem 21. Jahrhundert statistisch untersucht. Simulationen sind nötig, da lang-zeitliche, direkte Messungen des Auftriebs und dessen Variabilität schwierig sind. In den hier verwendeten Simulationen ist die Stärke des Auftriebs durch die simulierte vertikale Geschwindigkeit repräsentiert. Es wird angenommen, dass die vertikale Geschwindigkeit den Auftrieb direkter widerspiegelt als andere Variablen, die als Proxies verwendet werden. Diese Arbeit ist in drei Teile gegliedert, basierend auf den analysierten

Zeitperioden: die Gegenwart (1950-2010), die Vergangenheit (850-1849) und die Zukunft (2006-2100).

Das Upwelling der letzten 61 Jahre im Arabischen Meer wurde anhand einer hochaufgelösten globalen Ozeansimulation (10 km), angetrieben durch meteorologische Beobachtungen, analysiert. Die simulierte vertikale Geschwindigkeit zeigt einen Jahresgang mit Auftrieb von Mai bis September. Für diese Zeitperiode zeigt sich kein signifikanter Trend im Upwelling. Das Upwelling ist stark mit der Meeresoberflächentemperatur und dem küstenparallelen Windstress korreliert. Entgegen der momentanen Annahme sind die Korrelationen zwischen dem Upwelling und dem Indischen Monsun eher niedrig, was darauf schließen lässt, dass andere Faktoren für die Variationen des Auftriebs verantwortlich sind. Ich konnte ein Klimavariabilitätsmuster identifizieren, das sich von dem Muster, das den Monsun antreibt, unterscheidet und deutlicher zum Antrieb des Upwellings beiträgt. Zudem sind sowohl der Monsun als auch der Auftrieb mit einem ähnlichen Temperaturmuster verknüpft, allerdings sind die verantwortlichen Mechanismen für dieses Muster bei Monsun und Auftrieb verschieden.

Des Weiteren habe ich das Upwelling im Arabischen Meer des letzten Jahrtausends anhand von Simulationen zweier Erdsystemmodelle untersucht. Mit jedem Erdsystemmodell wurde ein Ensemble von drei Simulationen mit dem gleichen externen Forcing - aber anderen Anfangsbedingungen - durchgeführt. Dies führt dazu, dass der Einfluss des externen Forcings und der internen Variabilität separiert werden kann. Generell zeigen beide Modelle recht ähnliche Ergebnisse. Im Gegensatz zu den Ergebnissen aus dem ersten Teil zeigt sich für das letzte Jahrtausend ein klarer Zusammenhang, durch signifikante Korrelationen, zwischen dem Upwelling und dem Indischen Monsun. Der simulierte Verlauf des Upwellings stimmt mit dem aus Sedimentbohrkernen überein: ein negativer Langzeittrend zeigt sich in allen Simulationen dieser Zeitperiode. Das lässt darauf schließen, dass das externe Forcing für diesen Trend verantwortlich ist. Die Analyse des Luftdruckmusters in diesen Simulationen weist Ähnlichkeiten mit dem Luftdruckmuster im mittleren Holozän auf und lässt mich daher auf das orbitale Forcing als Antrieb für die Variabilitäten im Upwelling schließen.

Im letzten Teil dieser Doktorarbeit habe ich mich mit den Szenarien des zukünftigen Klimas und somit dem Klimawandel befasst. Dafür habe ich im Grunde die gleichen beiden Erdsystemmodelle analysiert wie im vorhergegangen Teil über das letzte Jahrtausend. Diese Simulationen zeigen eine Abnahme der Auftriebsintensität im RCP8.5 Szenario, dem Szenario mit dem stärksten Treibhausgasanstieg. Dies steht erst mal im Kontrast zu der Intensivierung der auftriebsförderlichen küstenparallelen Winde in diesem Szenario. Die Analyse des Vertikalprofiles des Auftriebs und der Meeresoberflächentemperatur lassen mich allerdings schlussfolgern, dass die verstärkte Schichtung der Wassersäule durch die Erwärmung des Arabischen Meeres die Upwellingintensität abschwächt. In den Szenarien mit einem schwächeren Anstieg der Treibhausgase in der Atmosphäre, wie dem RCP2.6 Szenario, zeigt sich kein signifikanter Trend, weder im Auftrieb noch im Wind. Diese Simulationen zeigen somit, dass sich die Antriebe für Trends im Upwelling in der Zukunft von denen, die das Upwelling heutzutage und in der Vergangenheit beeinflusst haben, unterscheiden können.

Küstenauftrieb ist ein kleinskaliger Prozess. Da diese Doktorarbeit hauptsächlich auf Klimasimulationen basiert, muss bei der Interpretation der Ergebnisse berücksichtigt werden, dass diese Simulationen aufgrund ihrer räumlichen Auflösung Defizite in Bezug auf das simulierte Upwelling aufweisen könnten. Deshalb sollten die Schlussfolgerungen in der Zukunft bestätigt werden, wenn diese Simulationen mit höher aufgelösten Modellen durchgeführt werden können.

Contents

CHAPTER 1
Introduction

1.1 Upwelling

The term upwelling describes the process by which water from deeper ocean layers is advected to the upper ocean layers closer to the surface of the ocean. The water masses below the ocean surface are usually cold and nutrient-rich so that when lifted by upwelling they cool the surface water and stimulate ocean biomass production (Robinson and Bauer 1976; Traganza et al. 1981; Kosro et al. 1991). Upwelling is normally triggered by the collaboration of the wind and the Earth's rotation. The rotation of the Earth generates the Coriolis force which pushes an object towards the right (left) of its moving direction in the Northern (Southern) Hemisphere. In the ocean, the wind driven water flow is affected by the Coriolis force, which results in a net transport perpendicular to the wind direction. This effect is known as the Ekman transport (Ekman 1905; Price et al. 1987; Rintoul and England 2002). In the Northern (Southern) Hemisphere, the Ekman transport drives the surface water away to the 90° right (left) of the wind direction (Fig. 1.1). Therefore, due to the conservation of mass, upwelling occurs as a

replacement of the surface water loss (Wooster et al. 1976; Pickett and Paduan 2003; Pardo et al. 2011).

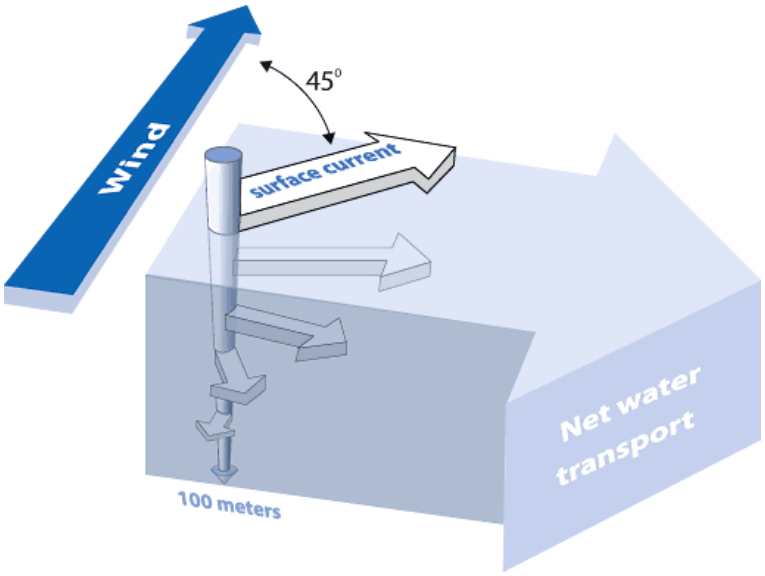

Figure 1.1: Demonstration of Ekman transport in the Northern Hemisphere. The surface water is divided into several layers. In the first layer the surface current moves 45° to the right of the wind direction as an effect of the Coriolis force and the drag forces. The water then moves to the right at a lower speed in each successive layer. Integrating all the layers will generate a net water transport to the 90° right of the wind direction (figure source: http://oceanservice.noaa.gov/education/kits/currents/media/supp_cur05e.html).

Based on the occurrence locations, upwelling can be categorized into open ocean upwelling and coastal upwelling. Open ocean upwelling is often associated with the divergence zones at the surface caused by winds or currents. There is a divergence of water mass at the surface water which is replaced by upwelled water mass beneath from deeper layers. One typical and most recognized open ocean upwelling area is along the equator where the easterly trade winds drag the surface water to move towards the west (Wyrtki 1981; Halpern and Feldman 1994; Johnson et al. 2001). Although the Coriolis force is weak in the tropics, the westward current is still

deflected by the Earth's rotation to the right in the Northern Hemisphere and to the left in the Southern Hemisphere. This causes a mass divergence that is filled by subsurface waters. Coastal upwelling shares the same basic mechanism with the open ocean upwelling as they both occur due to the advection of the surface water by the wind. In coastal regions, the upwelling is usually induced by the along-shore winds (Bakun 1973; Pedlosky 1978; Rutllant et al. 2004), which push the surface water offshore as the result of the Ekman transport and allow the subsurface water to rise (Fig. 1.2).

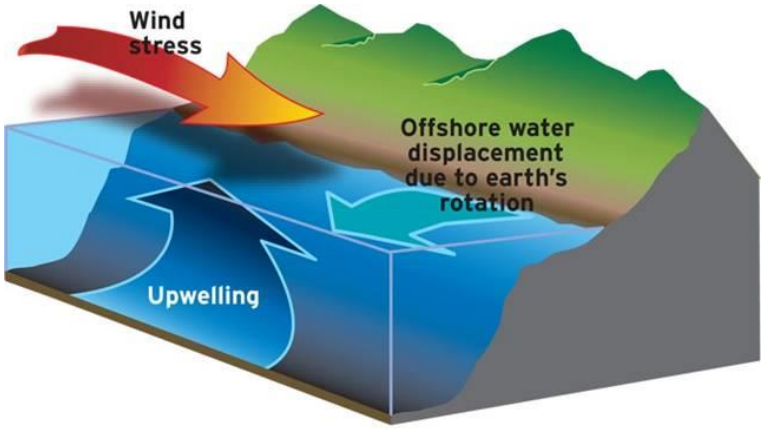

Figure 1.2: Mechanism of coastal upwelling in the Northern Hemisphere (figure source: https://www.nwfsc.noaa.gov/research/divisions/fe/estuarine/oeip/db-coastal-upwelling-index.cfm).

In this thesis I focus on the coastal upwelling because of its close relationship with human activities and its importance to the climate from regional to global scales. The most important coastal upwelling regions are located along the eastern boundaries of the main ocean basins as they benefit from the upwelling favourable winds associated to the permanent anticyclones over the mid-latitude oceans and from the eastern boundary currents (Philander and Yoon 1982; Bakun and Nelson 1991; Carr and Kearns 2003). The eastern boundary currents are the result of the large-scale wind climatology in interaction with the rotation of the Earth. These currents carry cold water from higher latitudes and flow towards the equator along the eastern side of the ocean

basins. Associating with the eastern boundary currents, there are four major Eastern Boundary Upwelling Systems (EBUSs): the California upwelling system off the western coast of North America (Huyer 1983), the Humboldt upwelling system off the western coast of South America (Chavez et al. 2008), the Canary upwelling system off the northwestern coast of Africa (Santos et al. 2005) and the Benguela upwelling system off the southwestern coast of Africa (Nelson and Hutchings 1983). They are located, respectively, in the areas of the California current, the Humboldt current, the Canary current and the Benguela current (Fig. 1.3). The nutrient-rich water mass that they lift to the surface marks these regions as the most biologically productive areas in the ocean. Covering less than 2% of the entire ocean area, the EBUSs support more than 20% of the global fish catches (Pauly and Christensen 1995).

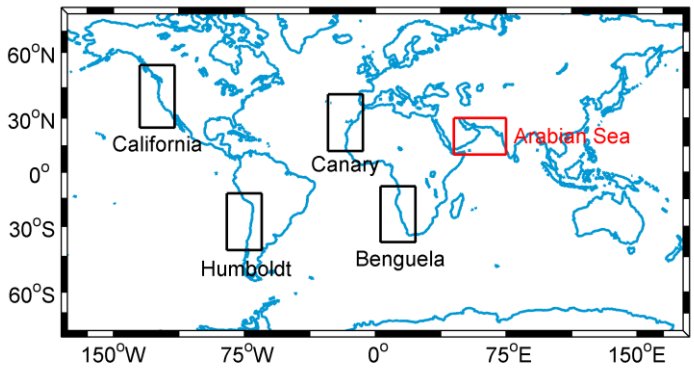

Figure 1.3: Locations of the major EBUSs and the Arabian Sea upwelling system.

It is suggested that upwelling in the major EBUSs will intensify as a result of the increased temperature gradient between the ocean and the land due to the effect of greenhouse gas forcing (Bakun 1990). Due to the thermal inertia of the ocean, surface temperatures will tend to increase more rapidly over land and this increasing thermal contrast between land and ocean will lead to an increased sea level pressure gradient between land and the ocean as well: the semi-permanent anticyclones located over the mid-latitude oceans would strengthen relative to the air pressure over the continents, leading to a strengthening of the coast-parallel wind conductive of upwelling.

This hypothesis has been widely tested but studies have presented diverging results (Sydeman et al. 2014; Varela et al. 2015; deCastro et al. 2016). The upwelling trends derived from these studies are shown to depend on the region, the time period and the data set used by the specific study. Although the basic physical mechanisms underpinning Bakun's hypothesis are sound, there may be other factors affecting upwelling intensity, like the stratification of the water column or even long-term internal variations due to ocean dynamics and not related to the external forcing. These additional sources of long-term variability of upwelling may blur the long-term trend potentially caused by the greenhouse gas forcing.

In addition to the major EBUSs, there is another ocean region of high biological productivity resulting from an intense coastal upwelling. This is the Arabian Sea. This region has different topological characteristics, as the Indian Ocean and the Arabian Sea are limited by west-east running land coastlines, in contrast to the north-south oriented coastlines in the other major ocean basis. This thesis is focused on upwelling in the Arabian Sea, with the aim of identifying the mechanisms that connect climate variability and trends with variability and trends in upwelling in this region.

1.2 Arabian Sea Upwelling

The Arabian Sea (Fig. 1.3) exhibits a very productive upwelling system in addition to the major EBUSs (Bauer et al. 1991; Banse and English 2000; Piontkovski et al. 2012). Basically upwelling in the Arabian Sea can be divided into two regions: upwelling in the western Arabian Sea along the coast of Oman (Prell and Curry 1981; Naidu and Malmgren 1996; Shi et al. 2000) and upwelling in the eastern Arabian Sea along the southwest coast of India (Banse 1959; Shetye et al. 1990; Smitha et al. 2008). My focus in this thesis lies on the coastal upwelling in the western Arabian Sea, and so hereafter the term Arabian Sea upwelling refers to the upwelling along the coast of Oman. Although located at the western boundary of the Indian Ocean, the Arabian Sea

upwelling is also mainly driven by the along-shore winds like the major EBUSs due to the effect of the Indian Monsoon (Bruce 1974; Anderson and Prell 1993; Tudhope et al. 1996).

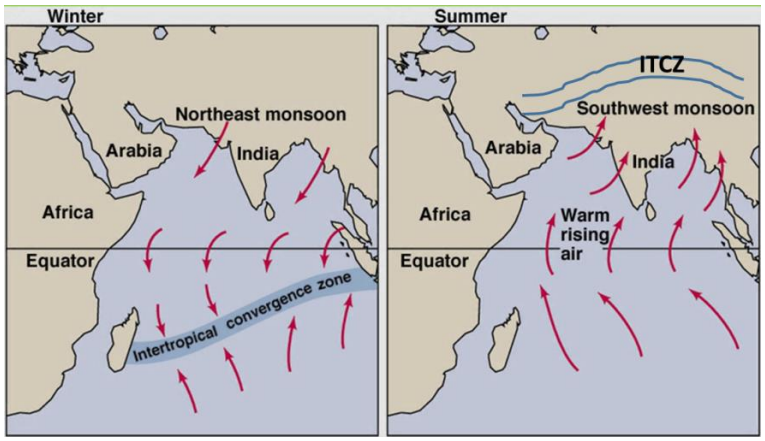

Figure 1.4: Diagram of the Indian Monsoon (figure source: http://iasmania.com/ climate-of-india/).

The Indian Monsoon is one of the most important climate features of annual and interannnual climate variability over Asia. The term Monsoon refers to the reversal of the direction of the prevalent seasonal winds from summer to winter every year (Fig. 1.4), which makes it a unique climate system (Clemens et al. 1991; Schott and McCreary Jr 2001; Gadgil 2003). During the boreal summer, the continuous heating rapidly raises the temperature in the Indian subcontinent forming a low pressure zone over this area. Meanwhile, the warming over the Indian Ocean is much slower than over the land, which causes a high pressure zone over the ocean. This strong pressure gradient between the land and the ocean results in southerly winds originating from as far as the southern Indian Ocean, and blowing to the Indian subcontinent. During winter, the land cools down faster than the ocean, and so a high pressure zone on the Indian subcontinent is formed and a low pressure zone over the Indian Ocean appears. Thus, the Indian Monsoon in winter reverses its direction and blows from northeast to southwest.

In summer, when the Indian summer Monsoon (ISM) dominates, the southwest wind blows almost parallel to the coast of the western Arabian Sea (Findlater 1969; Brock et al. 1992; Weller et al. 1998), which induces the offshore Ekman transport and thus the upwelling (Fig. 1.5). Therefore, the Arabian Sea upwelling has a strong seasonal cycle. It normally starts every year in May and ends in September (Brock et al. 1991). During summer, the upwelling lifts the water from depths below 200 meters beneath the ocean surface at a speed of about 2×10^{-5} m/s (Rixen et al. 2000) and causes a cooler water temperature by about 5.5 °C (Weller et al. 2002) in the sea surface temperature (SST).

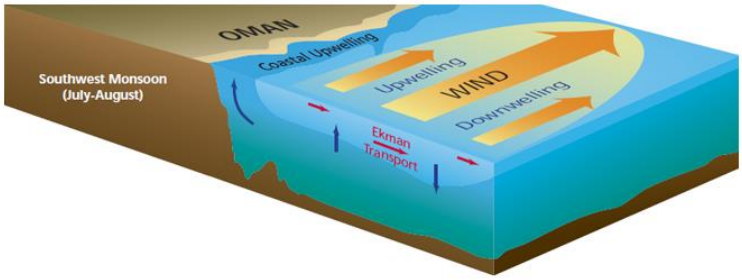

Figure 1.5: The formation of the Arabian Sea upwelling system (figure source: http://www.whoi.edu/services/communications/oceanusmag.050826/v40n2/weller.html).

The Arabian Sea upwelling is important due to the cold nutrient-rich water it brings to the surface (Fischer et al. 2002; Wiggert et al. 2002; de Boyer Montégut et al. 2007), which feeds the ocean biomass and thus contributes to the maintenance of fisheries. It is also of great scientific importance for understanding the climate variation because of its close relationship with the ISM (Schott 1983; Keen et al. 1997; Murtugudde et al. 2007). Many studies have generally linked the Arabian Sea upwelling and the ISM as the indicator of each other (Sirocko et al. 1991; Leuschner and Sirocko 2003; Anderson et al. 2010). On one hand, the ISM is believed to be the main driver of the upwelling as it causes the upwelling favourable wind, which in turn induces the Ekman transport that enables the upwelling. On the other hand, the upwelling may also have significant impact on the Monsoon and the associated rainfall over India, since it modifies the SST and

therefore the heat flux from the ocean to the atmosphere. A weakened upwelling increases the SST along the coast, and so the surface evaporation is enhanced. More water vapour is then transported to the land with the Monsoon through air-sea interaction, causing a strengthened rainfall over India. On the contrary, an intensified upwelling would reduce the Monsoon rainfall (Izumo et al. 2008). It is well known that the ISM brings moisture from the Indian Ocean to the Indian subcontinent and causes rainfalls there, which is essential to the local agriculture and economy.

Because of the unique characteristic of the Arabian Sea upwelling, it has attracted numerous studies. In terms of observations, scientists have used sediment records, satellite data, and ship observations which date back to the 19th century. Currie (1992) summarized and interpreted the data collected by several ship cruises from earlier times. That work described the vertical distribution of the water mass during upwelling and suggested that the Arabian Sea upwelling has features similar to the major EBUSs. Banzon et al. (2004) applied satellite ocean colour observations from SeaWiFS to study the Arabian Sea upwelling during May to September in 2000 whereas Liao et al. (2012) used the SeaWiFS data for the period from 1997 to 2009. In addition, Shi et al. (2000) employed satellite-derived sea level and SST data to study the Arabian Sea upwelling from 1993 to 1995.

The observations from ships and satellites are limited in temporal coverage and thus cannot provide a long-term view in the variability of the Arabian Sea upwelling. The sediment records, on the contrary, can be used to investigate upwelling from hundreds of thousands of years ago (Emeis et al. 1995; Naidu and Niitsuma 2003; Ishikawa and Oda 2007). It has been suggested, based on interpretation of sediment records, that the Arabian Sea upwelling has intensified during the past 400 years (Anderson et al. 2002; Feng and Hu 2005; Sinha et al. 2011). The reasons might be connected to the increased concentrations of greenhouse gases in the atmosphere but also to the increased solar activity over the past centuries. As explained before, the wind regime in the Indian Ocean is closely linked to the thermal contrast between the Indian Ocean and the Asian continent during spring and summer. These two types of forcings are able

to modulate the radiation balance at the surface and therefore could also be responsible for long-term trends in Arabian Sea upwelling. On longer timescales, the changes in the orbital parameters of the Earth's orbit also modify the seasonal and regional distribution of solar radiation impinging on the Earth surface and can therefore also influence the wind regime in the Indian Ocean.

Although the sediment records are able to cover these very long periods, they are normally collected from quite sparse locations, and may not be totally adequate to obtain information about the spatial variability of the upwelling. Therefore, it seems a good alternative to complement the study of the Arabian Sea upwelling by analysing the results obtained in simulations with simulated numerical models. However, a comprehensive model-based study focused on this issue is not yet available. One hurdle in these types of studies is the spatial resolution of the models used. Although the broad picture of mean coastal upwelling is well understood - as a result of along-coast wind-stress - upwelling may also be modulated by mesoscale ocean dynamics and by the small-scale wind variability. For instance, it has been observed that upwelling in the EBUSs presents a very rich small-scale (a few kilometers) spatial variability that results in a complex structure of filaments visible in the remote-sensed and in-situ analysis of chlorophyll (Lutjeharms et al. 1991; von Bodungen et al. 2008). On the other hand, state-of-the-art global ocean models used for multidecadal simulations have spatial resolution of the order of 100 km, which raises questions about their ability to properly represent upwelling dynamics. In addition, the ocean models have to be driven by either gridded meteorological reanalysis of wind-stress and surface fluxes or by high-resolution atmosphere models coupled to their ocean counterpart. The resolution of gridded meteorological reanalysis and atmosphere models nowadays is also of the order of 100 km, and although they are capable of properly capturing the large-scale structures of atmospheric dynamics, they may encounter problems to represent smaller scale turbulence at the interface between land and ocean.

This limitation is not easily overcome. Higher resolution simulations require either rapidly increasing computing capabilities or the limitation of the simulations to particular regions. In the

latter case, inconsistencies may arise between the higher resolved regions and the rest of the world ocean. An ideal simulation with a coupled atmosphere-ocean model with a spatial resolution of a few kilometres and running over several decades does not exist yet. The suitability of coarser resolution models to study long-term upwelling variability cannot be, however, ruled out. In this thesis, I have tried as much as possible to confront the models used with available observations, but there is a dearth of observational data to validate numerical models, so that it is difficult to prove or disprove the hypothesis that coarser resolution models are essentially inadequate.

Therefore, the present study, although admittedly analyses of state-of-the-art simulations that may not have the ideal spatial resolution to address upwelling dynamics, is nevertheless intended to contribute to its understanding, with the explicit caveat related to model resolution.

1.3 Thesis Objective

This study is part of the project of Universität Hamburg's Cluster of Excellence "Integrated Climate System Analysis and Prediction" (CliSAP) which is funded by the German Research Foundation (DFG). CliSAP aims to provide a platform where climate related studies can be jointly conducted by scientists specialized in various academic disciplines including meteorology, oceanography, ecology, sociology, economics, etc. The first phase of CliSAP ran from 2007 to 2012 which has been a great success and based on the experience the second phase (CliSAP-2) started in 2012 and will end in 2017.

This thesis is conducted within CliSAP-2 under the research topic "Marine and Coastal Systems" (B3) which mainly focuses on coastal upwelling systems and shelf sea systems of the northeastern Atlantic Ocean. As one of the major focuses, the evolution of the coastal upwelling systems from the past to the future and their responses to the climate change are studied by analysing model

outputs. Two upwelling regions are investigated: the southeastern Atlantic and the Arabian Sea. My interest here lies in the Arabian Sea and I statistically examine model results. By analysing the modelled upwelling velocity and comparing it with various oceanic and atmospheric variables, I try to answer the following research questions in this thesis:

- How close is the connection between the Indian Monsoon and the Arabian Sea upwelling modelled from a high resolution ocean simulation? Are there any trends indicating upwelling intensification over the last 60 years?

- How did the Arabian Sea upwelling evolve during the last millennium? How does the internal and external model forcings affect the results? What factors are responsible for the long-term variation of the upwelling?

- How will the Arabian Sea upwelling change in the future? What are the differences in the future upwelling when modelled under the weakest or the strongest greenhouse gas emission scenarios?

1.4 Thesis Outline

This thesis contains five chapters including the current introductory chapter and a concluding chapter in the end. Chapter 2, 3 and 4 are the main chapters which are designed to address the research questions, respectively. The three main chapters are connected and can also be read independently since they have been prepared separately for peer reviewed publications. A brief description of the main chapters is given as follows:

Chapter 2

I examine the relationship between the Arabian Sea upwelling and the ISM in an eddy-resolving global ocean simulation (STORM), which is driven by atmospheric reanalysis over the last 61 years. With its very high spatial resolution (10 km), STORM allows me to identify characteristics of the upwelling system. I analyse the co-variability between upwelling and meteorological and oceanic variables from 1950 to 2010. By using the modelled upwelling velocity, this study is a more direct approach compared to the studies based on upwelling proxies such as sediment records, SST and wind. The analysis reveals high interannual correlations between coastal upwelling velocity and along-shore wind-stress as well as with SST but low correlation between the upwelling and the ISM. I find that it is a different atmospheric circulation pattern from the one that drive the Monsoon the one that contributes to the upwelling variability. In spite of this, the patterns of near-surface air-temperature anomalies in South Asia that are either linked to Arabian Sea upwelling or to the Monsoon are spatially quite similar, although the physical mechanisms of these links are different. In addition, no long-term trend is detected in the modelled Arabian Sea upwelling as referring to the Bakun's hypothesis of upwelling intensification.

Chapter 3

The evolution of the Arabian Sea upwelling over the last millennium is investigated by studying and comparing the results from two earth system models: the Earth System Model of Max Planck Institute for Meteorology (MPI-ESM) and the Community Earth System Model (CESM). For each model, I examine an ensemble of three independent simulations which have the same external forcings but different initial conditions. In general, all the simulations present very consistent results in that the upwelling velocity is significantly correlated with the SST and the ISM. In addition, the modelled upwelling also shows quite good connection with the observational sediment records. A negative long-term trend is found in the upwelling velocity, which is very likely caused by the orbital forcing imposed on the model in the simulations.

Chapter 4

In this chapter I present the estimation of the Arabian Sea upwelling for the 21st century simulated under the greenhouse gas emission scenarios of Representative Concentration Pathway (RCP) 8.5 and RCP2.6 known as the strongest and the weakest scenarios. I apply the same models as in Chapter 3 but with slightly different model configurations specific for the future simulations. All the ensemble simulations are consistent on the future long-term trend under the RCP8.5 scenario. However, the upwelling exhibits a negative trend, whereas the southwest wind-stress increases, despite that fact that they are closely correlated at interannual timescales. Such phenomenon is not seen in the RCP2.6 scenario. This contrast between the two simulations indicates that the opposite trends in upwelling and southwest wind-stress result from the stronger greenhouse gas emission level. It is likely that under the RCP8.5 scenario the surface water stratification caused by the warming overrides the effect of the southwest wind-stress and thus hinders the upwelling.

CHAPTER 2

The relationship between Arabian Sea upwelling and Indian Monsoon revisited in a high resolution ocean simulation

2.1 Introduction

Coastal upwelling is important for ocean primary production as the upwelled cold nutrient-rich water supports coastal fisheries. In the Arabian Sea, one of the most important coastal upwelling regions along with the Eastern Boundary Upwelling Systems (EBUSs), upwelling is mainly controlled by the along-shore wind-stress during the summer season. It has been generally assumed that the variations of upwelling favourable winds in this region are connected to the variations of the Indian Monsoon (Findlater 1969). However, since there are little direct observations of ocean vertical velocity, it has been difficult to directly ascertain this link. In this chapter, I revisit this connection by analysing a very high-resolution ocean simulation with the model MPI-OM driven by meteorological reanalysis over the last decades.

Additionally, it has been hypothesized that coastal upwelling will strengthen in the major upwelling regions under the influence of global warming (Bakun 1990). In support of this hypothesis, Narayan et al. (2010) detected positive trends of upwelling intensity in the Canary, Benguela, California and Humboldt upwelling systems, which are known as the four major EBUSs. More recently Wang et al. (2015) projected the intensification of upwelling in three of the four major EBUSs (except for California) under a strong increase of anthropogenic greenhouse gas emissions. Bakun's hypothesis is related to the intensification of the land-ocean temperature gradient due to an intensification of the anthropogenic greenhouse gas forcing. I will also analyse to what extent the results from the simulation indicate an intensification of upwelling in the Arabian Sea over the past decades are compatible with this hypothesis.

The Arabian Sea upwelling and its relationship with the Indian summer Monsoon (ISM) have been widely investigated. Studies based on the abundance of the foraminifera *G. bulloides* from the sediment records intimately connected the Arabian Sea upwelling and the ISM (Anderson et al. 2002; Curry et al. 1992; Kroon et al. 1991; Prell and van Campo 1986). Since upwelling advects colder water masses to the surface, sea surface temperature (SST) is thought to be the most reliable indicator of the coastal upwelling in the Arabian Sea (Prell and Curry 1981) and it has been applied as a traditional upwelling index by various studies. More recently, Godad et al. (2011) reconstructed the SST from planktonic foraminifera and suggested that the peak upwelling season has shifted over the last 22,000 years in the western Arabian Sea. A comparison between the foraminifera collected from sediment traps in the western and the eastern Arabian Seas showed that the abundances were significantly correlated to the Monsoon but not to the SST and CO_2 (Naik et al. 2013). Emeis et al. (1995) used SST reconstructed from sediment records and Manghnani et al. (1998) processed SST from remote sensing data, while Izumo et al. (2008) combined modelled, in situ and satellite SST data, to derive an upwelling index. In addition, many studies have also used along-shore upwelling favourable wind-stress as another traditional upwelling index, as originally described by Bakun (1973).

These upwelling indices have been profusely used but they are not a direct measure of upwelling velocities. It is difficult to monitor vertical velocities over a long time span and, therefore, other studies have resorted to ocean simulations to study changes in the vertical velocity during upwelling. Recently, Jacox et al. (2014) analysed the vertical velocity from a four-dimensional regional ocean model to investigate the upwelling in the California current system. In the Arabian Sea, Shi et al. (2000) estimated the upwelling velocity off Oman from 1993 to 1995 through the combination of hydrographic and altimetry data. Anderson et al. (1992) employed a simple one-dimensional model to calculate the vertical upwelling velocity off Oman. Rao et al. (2008) used a three-dimensional model to compute the vertical velocity along the west coast of India. Studies applying ocean general circulation models also gave hints on the interaction of upwelling and SST (Ma et al. 2014) and the impact of Kelvin waves at the eastern boundary on the western Arabian Sea upwelling region (Tozuka et al. 2014). However, a study focused on the western Arabian Sea based on long-term four dimensional upwelling data is not yet available. In this chapter I try to fill this gap by employing the direct upwelling velocity data modelled in a high-resolution global ocean simulation over the period from 1950 to 2010. I compare the upwelling velocity with traditional upwelling indices (SST and wind-stress) and examine the relationship between the upwelling and the ISM as well as other potential factors that might affect the upwelling. An unexpected finding is that the correlations between the simulated upwelling and three different monsoon indices are low and non-significant, which indicates that over the past 61 years the impact of the ISM on the coastal upwelling in the western Arabian Sea could have been weaker than previously thought and that other large-scale atmospheric forcing is a more efficient driver of upwelling in this region.

2.2 Model and Data

The German consortium project STORM is aimed at developing high-resolution global climate change simulations. The ocean model simulation used in this chapter is hereinafter referred to as

the STORM simulation, which is described in von Storch et al. (2012). It is based on the Max-Planck Institute Ocean Model (MPI-OM) forced by the 6-hourly National Center for Environmental Prediction (NCEP) / National Center for Atmospheric Research (NCAR) reanalysis (Kalnay et al. 1996) for the period from 1948 to 2010. The model's original bipolar grid is replaced by a tripolar grid to obtain an isotropic horizontal resolution. Comprising 3602 × 2394 horizontal grid points in total, the STORM simulation has a horizontal resolution of 0.1° around the equator but coarser towards the poles. On the vertical direction, the STORM simulation has 80 levels which are extended to over 6000 m and in the upper 200 m the levels are separated by 10 to 15 m.

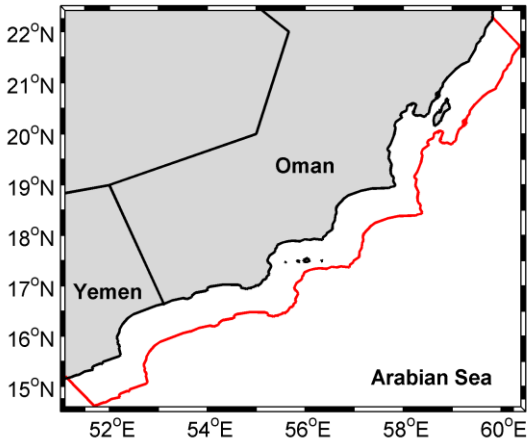

Figure 2.1: The main study area with the selected coastal upwelling region demonstrated by the red line.

Upwelling velocity is derived from the vertical water mass transport in the STORM simulation output. The high spatial resolution of the STORM simulation allows me to capture the upwelling variability on small scales. The chosen upwelling domain (Fig. 2.1) extends about 90 km offshore along the coast of Yemen and Oman between 15.2°N to 22.3°N (Rixen et al. 2000). According to Brock and McClain (1992), I average the upwelling velocity over the upper 200 m of water. I

compare the upwelling velocity derived from the STORM simulation with observational SST and wind-stress derived from different sources. SST data are obtained from the Advanced Very High Resolution Radiometer (AVHRR) Pathfinder Version 5.0 (Casey et al. 2010). Wind data are provided by the NCEP/NCAR reanalysis and the Cross-Calibrated Multi-Platform (CCMP) project (Atlas et al. 2011). The area selected for calculation of the wind data time series is the entire ocean domain in Fig. 2.1.

Since different wind datasets are applied and compared here, for the sake of consistency I calculate the wind-stress from the wind datasets instead of using directly the native wind-stress to avoid any bias between the algorithms used to derive the wind-stress by different projects. The along-shore upwelling favourable wind-stress is calculated as:

$$\boldsymbol{\tau_{SW} = \rho \cdot C_D \cdot \sqrt{u^2 + v^2} \cdot (u \cdot cos\alpha + v \cdot cos\beta)}$$

where $\boldsymbol{\rho}$ is the air density which is assumed as 1.22 kg m^{-3} and the drag coefficient $\boldsymbol{C_D}$ is computed using the formulation of Yelland and Taylor (1996); $\boldsymbol{u}$ and $\boldsymbol{v}$ are the zonal (eastward) and meridional (northward) wind speed components respectively; $\boldsymbol{\alpha}$ and $\boldsymbol{\beta}$ are the angles between the wind speed components and the coastal orientation and in this case both of them are assumed to be 45° because of the orientation of the coast in the study area.

The monsoon intensity has been defined by different climate indices that capture different aspects of the monsoon variability. Here, I use monsoon indices taken from the literature that are based on low-tropospheric winds over South Asia or Indian precipitation. With this analysis, however, I do not imply that precipitation, for instance, may be a direct driver of Arabian Sea upwelling. In order to estimate the statistical relationship between upwelling and the Monsoon, I employ the wind-based Indian Monsoon index (IMI) defined by Wang and Fan (1999) and the All India Monsoon rainfall index (IMR) from the Indian Institute of Tropical Meteorology (IITM) introduced by Parthasarathy et al. (1994) as well as the Webster and Yang monsoon index (WYM) defined by Webster and Yang (1992) which is also defined in terms of wind speed. I calculate the IMI and WYM based on wind speed from NCEP/NCAR reanalysis while the IMR is obtained

from station rainfall records in India. Figure 2.2 shows the domains used for calculating the IMI and the WYM indices. The IMI is obtained by subtracting the averaged zonal wind speed at 850 hPa (U850) in box 2 (70°E – 90°E / 20°N – 30°N) form the averaged U850 in box 1 (40°E – 80°E / 5°N – 15°N). The WYM is calculated by subtracting the averaged zonal wind speed at 200 hPa (U200) from U850 in the shaded box 3 (40°E – 110°E / 0°N – 20°N).

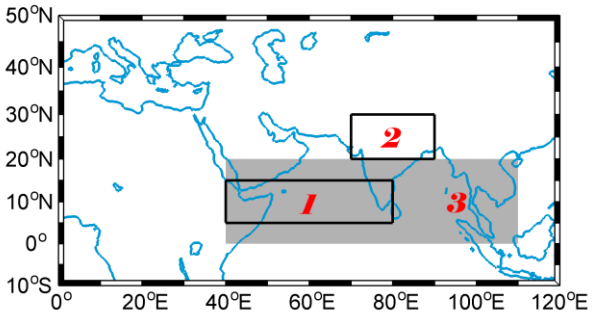

Figure 2.2: Wind speed domains selected for calculating the IMI and WYM indices where the box 1 and box 2 are for IMI and the shaded box 3 is for WYM.

In addition, several other meteorological and oceanic variables are also investigated. Surface air temperature (ST) data and sea level pressure (SLP) data from the NCEP/NCAR reanalysis are investigated to provide further understanding. Because of a continuity issue in the STORM simulation output (missing data in year 1949), I limit the study period from 1950 to 2010. The only datasets not covering this whole period are the AVHRR SST data (1985-2009), CCMP winds (1988-2010), and the IMR record (1950-2000). Table 2.1 lists the details of all the data employed in this chapter.

Table 2.1: Information for data used in Chapter 2. *All India Monsoon rainfall index (IMR) from the Indian Institute of Tropical Meteorology (IITM).

Variable	Data Source	Resolution	Temporal Coverage
Upwelling Velocity	STORM	0.1° / 10 km	1950 - 2010
SST	STORM	0.1° / 10 km	1950 - 2010
	AVHRR	0.04° / 4 km	1985 - 2009
Wind Speed	NCEP/NCAR	2.5° / 250 km	1950 - 2010
	CCMP	0.25° / 25 km	1988 - 2010
MLD	STORM	0.1° / 10 km	1950 - 2010
SLP	NCEP/NCAR	2.5° / 250 km	1950 - 2010
ST	NCEP/NCAR	2.5° / 250 km	1950 - 2010
IMR*	IITM		1950 - 2000

Since the model has already been globally analysed and assessed (von Storch et al. 2012), I hereby present the information of the modelled mixed layer depth (MLD) and the comparison between the modelled SST and the observational SST from AVHRR. Figure 2.3 shows that the simulated MLD is shallower along the coast than in the open sea and that the MLD in the upwelling region is slightly deeper during the upwelling season than during the pre- or post- upwelling season, although the mixed layer is clearly deepest during the winter season. That the MLD attains a relative maximum during the upwelling season is a reasonable result as described by Murtugudde et al. (2007). The shallowing of MLD caused by upwelling is counteracted by strong surface turbulent kinetic energy and entrainment cooling, which tend to deepen the MLD.

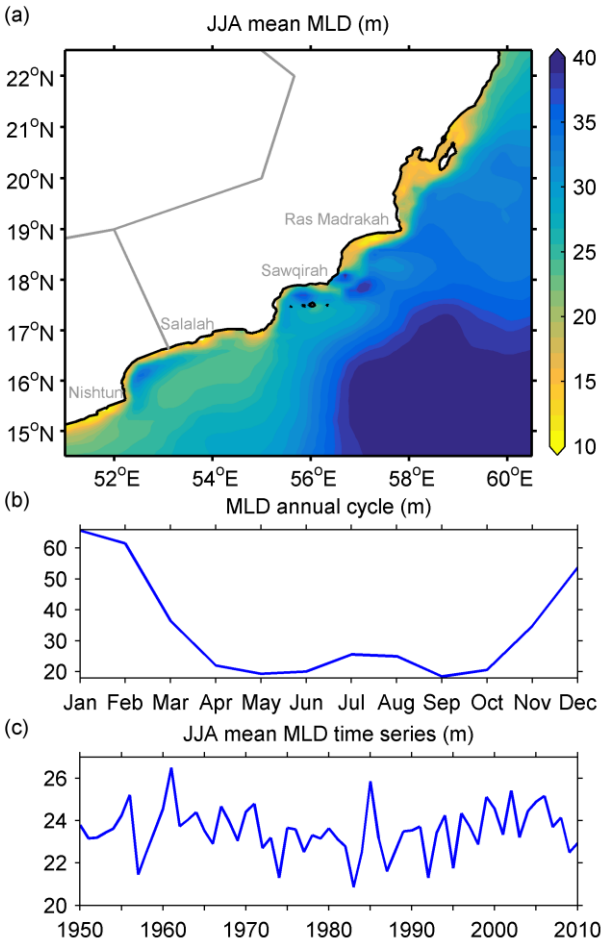

Figure 2.3: (a) Summer mean MLD (m) from 1950 to 2010. (b) Annual cycle of MLD (m) in the study area. (c) Time series of summer mean MLD (m) in the study area (1950-2010).

The SSTs from STORM and AVHRR are compared in Fig. 2.4. In general, the SST from STORM is cooler than that from AVHRR in the upwelling region but they display good correlation (r=0.51) and even better correlation in the open sea, which indicates that the model is capable to simulate the observed variabilities.

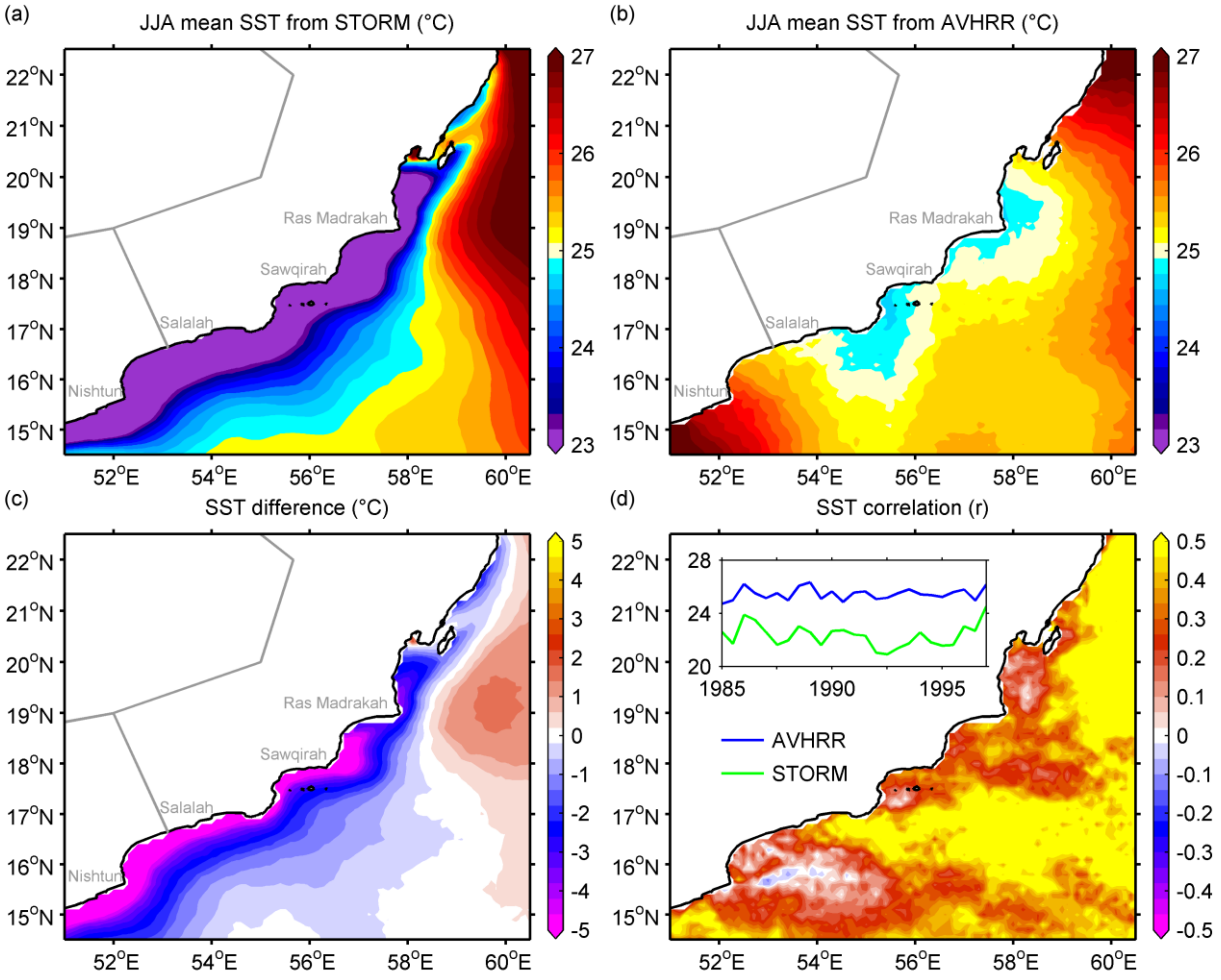

Figure 2.4: (a) Summer mean SST (°C) from STORM. (b) Summer mean SST (°C) from AVHRR. (c) Summer mean SST difference (°C) between STORM and AVHRR. (d) Summer mean SST correlation (r) between STORM and AVHRR. The time period is chosen from 1985 to 2009 to be consistent with AVHRR. The plot in (d) shows the 25-year time series of the summer mean SSTs (°C) from STORM and AVHRR in the study area.

2.3 Western Arabian Sea coastal Upwelling

2.3.1 Upwelling annual cycle

Upwelling along the west coast of the Arabian Sea usually starts in May and ends in September (Brock et al. 1991). This is well reproduced in the modelled annual cycle of the upwelling velocity (Fig. 2.5a), which is converted from the original model output of upward water mass transport. Here, positive values indicate upwelling whereas negative values indicate downwelling.

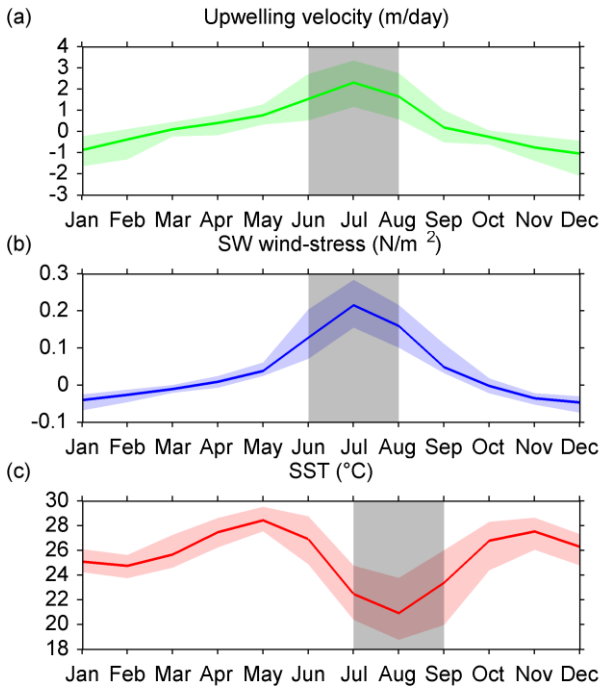

Figure 2.5: Annual cycle of (a) upwelling velocity (m day^{-1}), (b) SW wind-stress (N m^{-2}) and (c) SST (°C) averaged for the study area. Colour shaded areas are the ranges of the annual cycles and grey shaded months are the study periods selected for each variable.

The annual cycle of the upwelling velocity shows that the significant positive values start from May, peak in July and end in September. As one of the traditional upwelling indices, the south-west (SW) wind-stress (Fig. 2.5b) is in good consistency with the upwelling velocity with a peak in July as well. Another traditional upwelling index is the observed coastal SST. The modelled SST (Fig. 2.5c) also reveals good correlation with the upwelling velocity with a lag of approximately one month. This lag can be explained by the time needed to transport deeper and cooler water to the surface and it matches a similar lag between wind-stress and SST found in the observations by Rixen et al. (2000). It is obvious that the ranges of these three annual cycles tend to get larger when the upwelling becomes stronger. Therefore, unless indicated otherwise, when referring to summer period in the following analyses, I average the values from June to August (JJA) for all the variables except SST which is selected from July to September (JAS) due to the previously mentioned time lag.

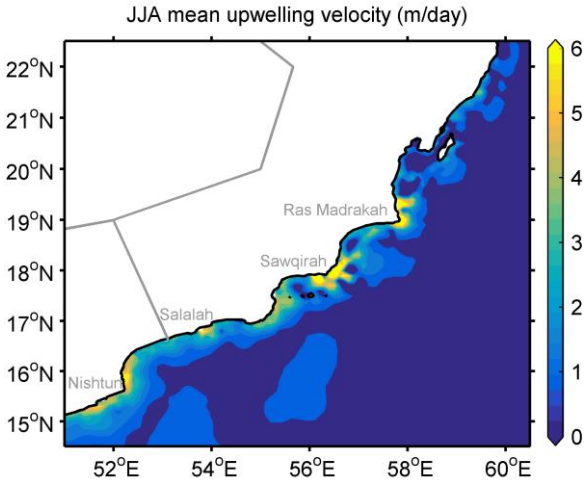

Figure 2.6: Summer mean upwelling velocity averaged over the upper 200 m of water in the study area.

The selected coastal upwelling band (Fig. 2.1) is very narrow but the high resolution of the STORM simulation means it can reproduce the spatial patterns of the upwelling in the study

domain. Figure 2.6 reveals that the simulated mean upwelling velocity averaged over this domain in JJA from 1950 to 2010 is about 1.8 m day^{-1}. Upwelling is less intense in the area north to Ras Madrakah and much stronger at regions near the capes such as Sawqirah and Nishtun where the velocity can exceed 6 m day^{-1} at some model grid-cells. These velocities appear compatible with the estimation of the high range of the vertical velocity estimated by Shi et al. (2000) from altimetry data of about 2.5 m day^{-1}, considering the coarser resolution of the satellite data relative to the ocean model.

2.3.2 Upwelling trend

My primary attempt is to investigate any long-term trend in the upwelling time series referring to the Bakun hypothesis (Bakun 1990) that coastal upwelling should intensify as a consequence of anthropogenic greenhouse gas forcing at global scale. This hypothesis has been contested and recent studies have shown both supportive (Sydeman et al. 2014) and unsupportive (Tim et al. 2015) results as regards the long-term trends. In My study, however, only a non-significant positive trend (p-value = 0.1954) is revealed over the last 61 years (Fig. 2.7a). This trend has a slope of 0.0035 m day^{-1} per year, which over the 60 years of simulation would imply an increase of about only 12% of the mean coastal upwelling velocity in the domain. Hence, although the trend may physically exist, it cannot be distinguished from a spurious trend caused by stochastic variability. Thus I do not further discuss about trends in the following text. However, although the trend is not statistically significant due its magnitude relative to the interannual variability and to the short length of the simulation, I detrend all variables in the subsequent correlation analysis to avoid that these correlations maybe contaminated by long-term trends that might not necessarily be physically related.

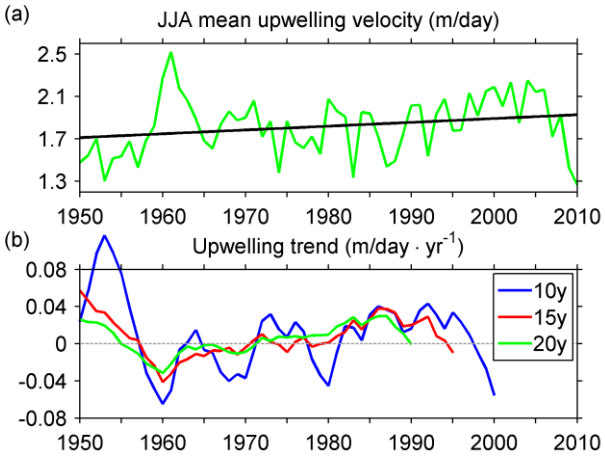

Figure 2.7: (a) Time series of summer mean upwelling velocity (green) and its long-term trend (black) from 1950 to 2010. (b) Decadal trends of upwelling velocity calculated for 10 years (blue), 15 years (red) and 20 years (green). The years on the x-axis correspond to the beginning years of the trend calculations.

Despite of the fact that no significant long-term trend can be detected, I notice the possible existence of decadal trends. For instance, in Fig. 2.7a it is clear that upwelling velocity increased significantly from 1950s to 1960s, followed by a drop until the mid-1980s and then it rose again before it fell again at around 2005. Thus, I calculate the decadal trends of different lengths from my upwelling time series (Fig. 2.7b). The set of the 10-year trends has the largest variation and it capture the largest trend in the beginning of the time series resulting from the extremely high value of upwelling velocity at around 1960. The 15-year and 20-year trends fail to capture this because of the time span used to calculate the trends, which exceed the time when the extreme value occurred. Nevertheless, the 15-year and 20-year trends are quite consistent with each other and they both indicate the increase in the trends from 1960 to 1985 and the decrease afterwards. In this increasing period, an apparent 10-year cycle is revealed in the 10-year trends, where the values of the trends are relatively lowest at 1960, 1970 and 1980. The decadal trends show that the upwelling velocity varies much in the last 61 years with both positive and negative trends in

all the time lengths I have studied but the variation is more stable in longer timescales (15-year and 20-year).

2.3.3 Upwelling variability

For an understanding about the spatial variability of upwelling in this region, I calculate the standard deviation (STD) and perform an Empirical Orthogonal Function (EOF) analysis (von Storch and Zwiers 2001) of the upwelling velocity. The STD map (Fig. 2.8a) shows that higher mean intensity of upwelling comes with higher variance, that is, in the regions where the upwelling velocity is higher (Fig. 2.6), the STD of the upwelling velocity is also higher. The mean STD over the entire study area is about 0.7 m day^{-1}, which is nearly half of the mean upwelling velocity.

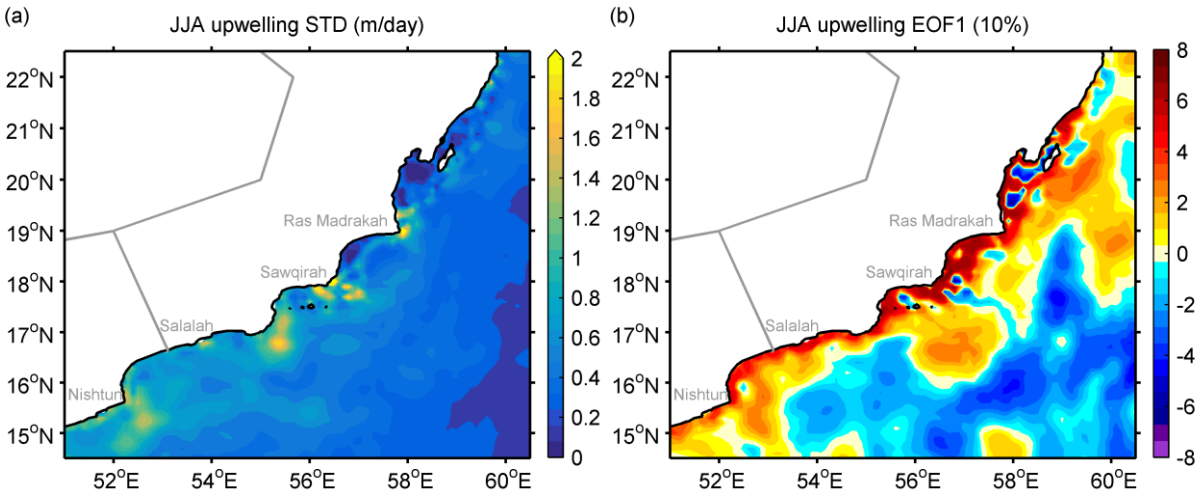

Figure 2.8: (a) Summer mean upwelling velocity STD (m day^{-1}) from 1950 to 2010. (b) Leading mode of the EOF analysis of the summer mean upwelling velocity which accounts for only 10% of the variance.

The EOF analysis is a method that identifies the main spatial patterns of coherent variation. This method identifies spatial patterns that describe most of the data variance and that display uncorrelated temporal evolutions. In my case, the leading EOF mode arising from the analysis (Fig. 2.8b) reveals apparent coastal-offshore pattern and accounts for only 10% of the total variance. The first principal component (PC1) time series is highly consistent with the spatially averaged upwelling velocity ($r = 0.82$, shown in Fig. 2.9a). However, the high STD with respect to the mean value of upwelling velocity and the low explained variance from the leading mode of the EOF analysis together indicate that the upwelling in this region is spatially very heterogeneous and must be affected by various and complex processes. A dominating influence by one single mechanism, for instance, the Monsoon, would give rise to a leading pattern describing a much higher portion of variance. This spatially heterogeneous variability of simulated upwelling confirms the findings derived from surface chlorophyll concentrations as an indirect indicator of upwelling (Piontkovski and Al-Jufaili 2013) and modelling results with a high-resolution regional model (L'Hégaret et al. 2015). The high mesoscale variability mainly arises in that model simulation by the generation of Rossby waves along the Indian coast, which may affect the upper 1000 meters in that model. Although the detailed analysis of the mesoscale variability in the STORM simulation is outside the scope of the present study, it is reasonable to assume that the high spatial variability in STORM in this region may be generated by similar mechanisms.

Beside the spatial variability, I also look at the temporal variability of upwelling. I compare the time series of the upwelling velocity with SST and the SW wind-stress to validate the modelled upwelling data since they are generally applied as coastal upwelling indices (Fig. 2.9). The time series of upwelling and SST are generated using data within the upwelling domain shown in Fig. 2.1 while the SW wind-stress time series contains data from a broader area due to the low resolution of the wind data. In Fig. 2.9a, the upwelling velocity and the PC1 time series from the EOF analysis are compared with SST from the STORM simulation and the SW wind-stress from the NCEP/NCAR reanalysis. The comparison reveals that the upwelling is strongly negatively correlated to the SST ($r = -0.83$) as well as positively to the SW wind-stress ($r = 0.73$).

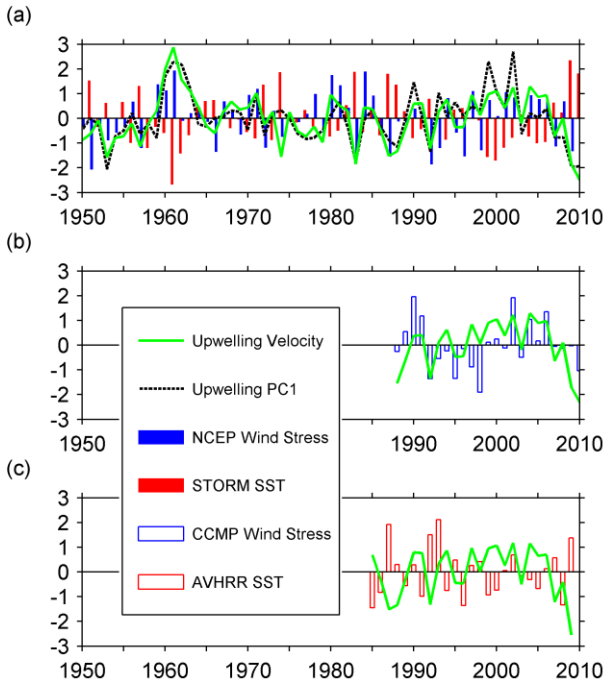

Figure 2.9: (a) Time series comparison of summer mean upwelling velocity, upwelling PC1, SW wind-stress from NCEP and SST from STORM (1950-2010). (b) Time series of summer mean upwelling velocity and SW wind-stress from CCMP (1988-2010). (c) Time series of summer mean upwelling velocity and SST from AVHRR (1985-2009). All the time series are calculated by averaging the values within the study area and are detrended and normalized for their spanning time periods.

Since the SST and the upwelling velocity are both outputs from the STORM simulation and the NCEP wind data is the forcing used in this simulation, these high correlations are to some extent expected and less persuasive without the support from extra sources. Therefore, I employ wind data from CCMP and SST data from AVHRR (Fig. 2.9b and 2.9c) as they are independent of the STORM simulation, although their temporal coverages are shorter than STORM. The correlations between simulated upwelling and these two observed variables are lower (wind r =

0.49 and SST r = -0.45) but they remain significant at the 95% level or higher as in the previous analysis.

These analyses suggest that the results of the STORM simulation are rather consistent with the observations, and more importantly, the upwelling velocity derived from the STORM simulation is significantly consistent with the traditional upwelling indices, and so it is reasonable to use it for further studies such as investigating the responsible processes affecting the upwelling.

2.4 Connections between Upwelling and its possible responsible factors

2.4.1 Link to the Indian Monsoon

As it has been suggested that the ISM is strongly linked to upwelling in the western Arabian Sea, I examine the relationship between the simulated upwelling velocity and the Indian Monsoon index (IMI), all India Monsoon rainfall index (IMR) and Webster and Yang monsoon index (WYM) in Fig. 2.10. Note that the IMR is computed by integrating the total rainfall records of numerous stations from June to September (JJAS) and the data source is not available for single months. Thus, I calculate the IMI and the WYM and also the upwelling velocity for the extended JJAS season.

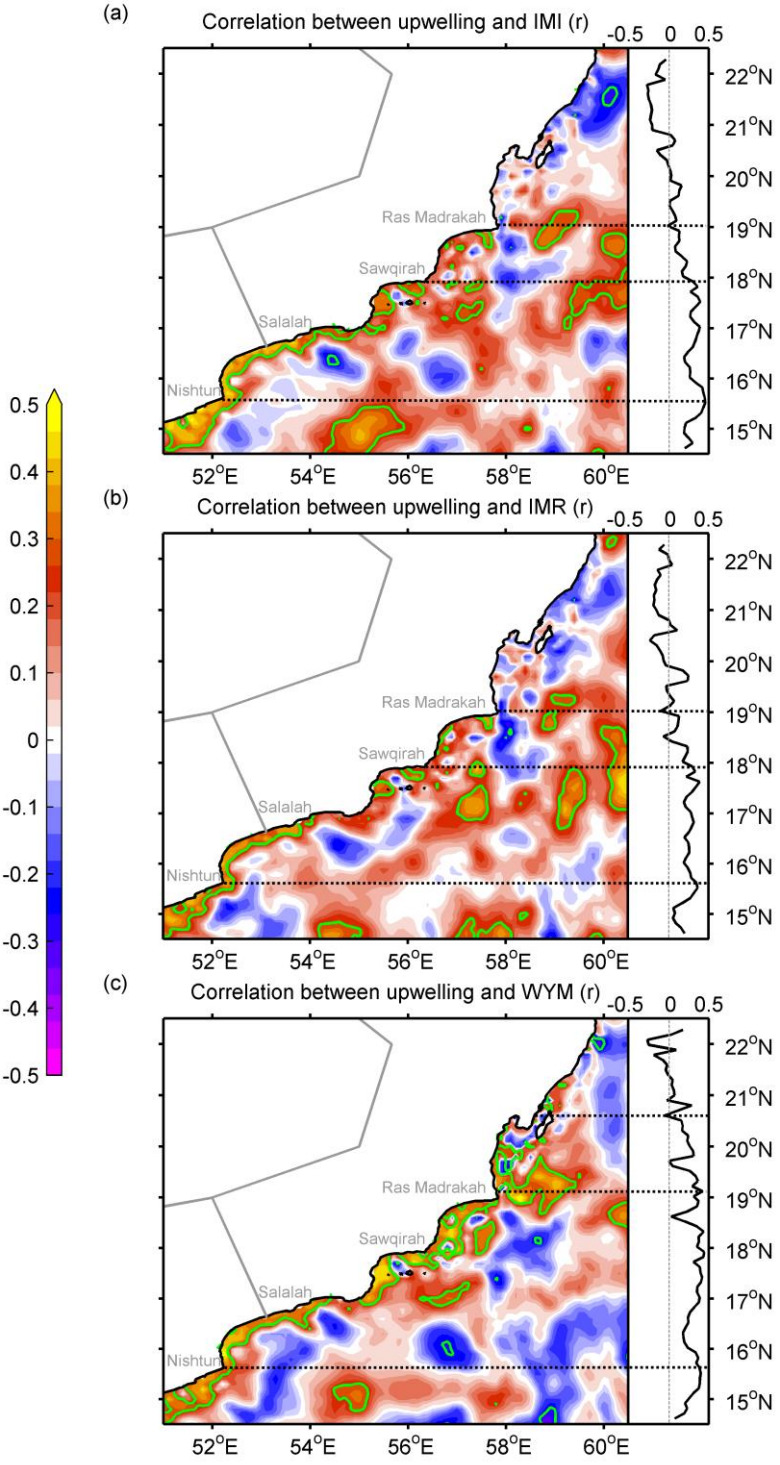
(a)
Correlation between upwelling and IMI (r)
(b)
Correlation between upwelling and IMR (r)
(c)
Correlation between upwelling and WYM (r)
-0.5 0 0.5
Ras Madrakah
Sawqirah
Salalah
Nishtun
22°N
21°N
20°N
19°N
18°N
17°N
16°N
15°N
52°E
54°E
56°E
58°E
60°E
0.5
0.4
0.3
0.2
0.1
0
-0.1
-0.2
-0.3
-0.4
-0.5

Figure 2.10: Correlations (r) between summer mean upwelling velocity and (a) IMI, (b) IMR as well as (c) WYM indices. Within the green contours are the areas where the significant levels are 95% or higher. The plots to the right of each map show the meridional mean correlation coefficient between each monsoon index and the summer mean upwelling velocity averaged within the study area. The upper dashed lines indicate the general starting points of the positive correlations and between the middle and the lower dashed lines are the areas where the correlations are the highest.

All of the three comparisons show low and negative correlations in the northern part of the domain. Higher correlations are found along the coast and to the south especially the regions with more intense upwelling and larger variance, but only a few areas show correlations that pass the significance level of 95%. One interesting finding is that the correlation patterns obtained with IMI (Fig. 2.10a) and with IMR (Fig. 2.10b) are quite similar. The correlations start to become positive at Ras Madrakah and the highest and the most significant correlations are located between Sawqirah and Nishtun. In addition, the areas with stronger correlation and higher significance strongly overlap. Considering the fact that IMI is calculated from the difference of two wind-speed fields whereas IMR is obtained from the rainfall records, this similarity indicates that the upwelling has very similar link to the variation of the wind-speed and the rainfall. These links likely arise through the large-scale patterns that drive climate anomalies in this region, but do not imply that rainfall is a dynamical driver of upwelling.

The WYM correlation pattern (Fig. 2.10c) shows a different structure, with positive values that begin to appear from the north of Ras Madrakah and the strongest and most significant correlation lies between Ras Madrakah and Nishtun. Although WYM is also calculated from the difference of two wind-speed fields, the strategies for selecting the fields are not the same and this is causing the difference between the patterns of IMI and WYM. Additionally, the two wind-based indices, IMI and WYM, capture reduced correlations near Salalah but IMR does not.

The spatially heterogeneous correlations indicate that the upwelling velocities in different regions along the western Arabian Sea coast are sensitive to different forcing mechanisms. Furthermore, it is surprising that the overall correlations of upwelling with all monsoon indices are rather low and non-significant. With regards to the STORM simulation, therefore, this analysis indicates that the impact of the ISM on western Arabian Sea coastal upwelling is weak and limited to areas with upwelling of higher intensity (Fig. 2.6) and variability (Fig. 2.8a).

2.4.2 Relationship with sea level pressure

In order to determine the other possible large-scale atmospheric patterns that could influence the variability of upwelling, I study the SLP (Fig. 2.11) and ST (Fig. 2.12) field in the broader Asian (Indian Ocean) region. SLP and ST are both reported to be highly associated with the ISM although their relationships with upwelling have not been directly studied yet. Figure 2.11a shows the mean summer SLP, with the low pressure zone over the Arabian Sea and Indian subcontinent is surrounded by the high pressure zones. The gradient between the high pressure and the low pressure zones contributes to the formation of the ISM. The leading mode of the EOF analysis of SLP (Fig. 2.11b), which describes a large part of the SLP variability (61%) indicates that the variation of SLP over the ocean and the continent tend to be in phase, which means the variability of the ocean-continent SLP gradient is not large. The first principal component from the EOF analysis of upwelling, PC1 will be used as an index of upwelling in the following analyses. In Fig. 2.11c I correlate the PC1 with the SLP field to gain an insight between the relationship of the upwelling variability and the SLP field. The pattern of correlations displays the positive correlations over the Arabian Sea and the negative correlations over the Himalayas.

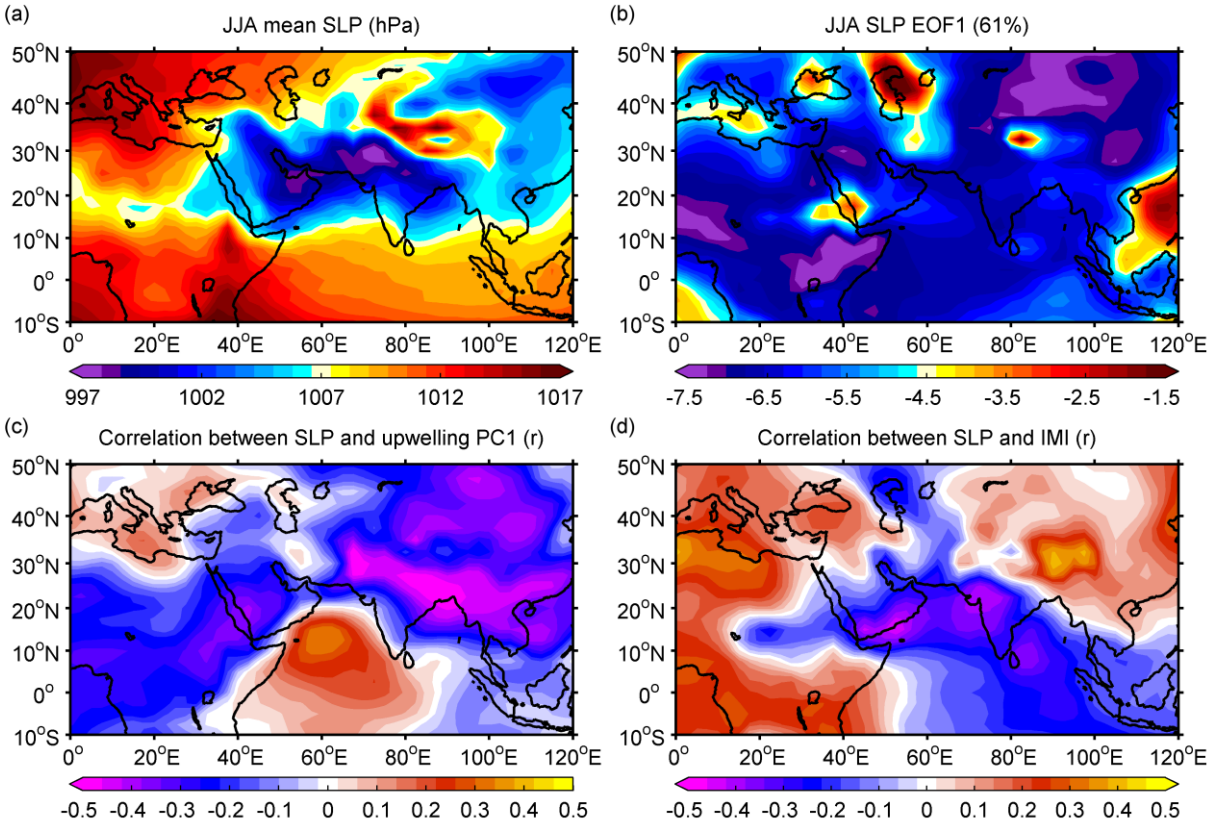

Figure 2.11: (a) Summer mean SLP (hPa) from 1950 to 2010. (b) Leading mode of the EOF analysis on the summer mean SLP which accounts for 61% of the variance. (c) Correlation (r) between upwelling PC1 and summer mean SLP. (d) Correlation between IMI and summer mean SLP.

I also take one of the monsoon indices, the IMI, to correlate with the SLP field (Fig. 2.11d). With negative correlations over the Arabian Sea and positive correlations over Himalayas, the IMI shows different connections with the SLP field compared to the correlation pattern derived from the upwelling PC1. Thus, the upwelling PC1 is well correlated to the SW wind generated by the gradient of the SLP field, which is also found in Subsection 2.3.3. However, in contrast to the upwelling PC1, the IMI is not linked to this gradient, which might explain the poor correlation between upwelling and the monsoon indices found in Subsection 2.4.1.

2.4.3 Relationship with surface air temperature

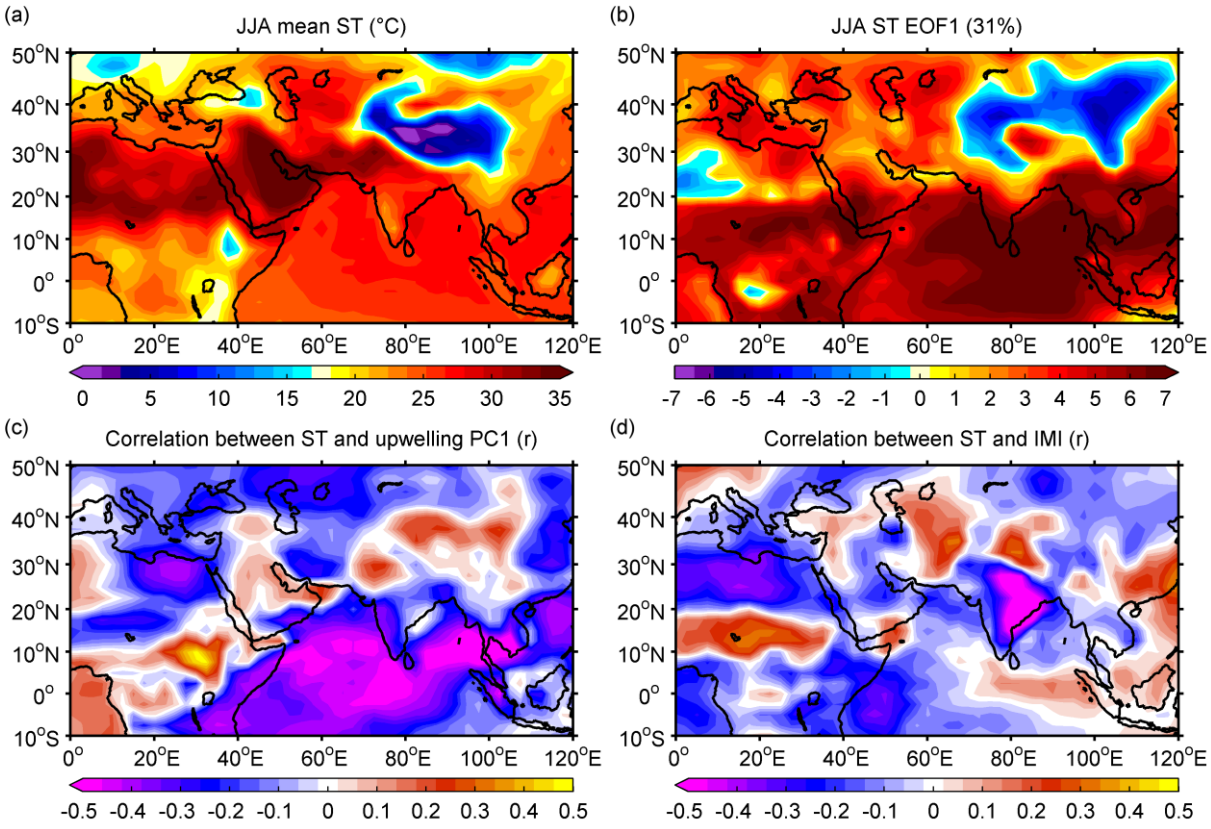

Figure 2.12: (a) Summer mean ST (°C) from 1950 to 2010. (b) Leading mode of the EOF analysis on the summer mean ST which accounts for 31% of the variance. (c) Correlation (r) between upwelling PC1 and summer mean ST. (d) Correlation between IMI and summer mean ST.

Since the seasonality of the Indian Monsoon is thought to be mainly driven by the temperature contrasts between land and Indian Ocean, the same analysis is performed on the ST field. The JJA mean ST map (Fig. 2.12a) shows that the lower temperature dominates the Tibetan Plateau, where also the high SLP is located (Fig. 2.11a). The leading EOF mode of ST (Fig. 2.12b) shows

that the temperature in northern India and temperature in central India tend to be anticorrelated. The correlation patterns between ST and upwelling PC1 (Fig. 2.12c) and the correlation between ST and IMI (Fig. 2.12d) also reveal correlations of opposite signs in these two regions. Thus, according to the EOF analysis, in the years in which the central Indian is colder than northern India, the upwelling and the ISM tend to be more intense. The upwelling PC1 has a similar link to the ST as the IMI although the IMI has more significant correlations. Thus, the relationships between upwelling and temperature and the ISM and temperature are much more similar than in the case of SLP.

Therefore, I have found that upwelling and Monsoon are connected to different SLP patterns, but both are linked to similar temperature patterns over this part of Asia. This can explain why upwelling may have been considered in the past to be closely related to the Monsoon. The physical explanation that I suggest here is that the SLP pattern related to upwelling is physically linked to stronger westerly winds over the Arabian Sea and a stronger advection of maritime air masses from the Arabian Sea into the Indian subcontinent, causing lower temperatures there. In contrast, as it is well known, the Monsoon is connected to higher rainfall over India, with increased cloudiness, less solar radiation, and therefore also lowers temperatures over the Indian subcontinent. Thus, the physical reasons for the lower temperatures in India in years with stronger Monsoon and in years with stronger upwelling are physically different. The same physical reasoning can be applied in years with weaker upwelling or weaker Monsoon, respectively.

2.5 Discussion and Conclusions

In this chapter I use the upwelling simulated by a high-resolution global ocean simulation over the past decades to identify the atmospheric drivers of upwelling along the west coast of the

Arabian Sea. With significantly improved spatial resolution, the modelled upwelling velocity presents consistent annual cycle with the traditional upwelling indices.

One limitation of my study that has to be borne in mind is the degree of realism of the ocean model used. Another possible limitation is the realism of the atmospheric forcing (NCEP/NCAR meteorological reanalysis) used to drive the ocean model. It is difficult to validate the simulated upwelling against direct observations of vertical velocities, and thus I have to rely on indirect analysis. Here, I show that the link between simulated upwelling and SSTs, and the correlation between simulated upwelling and independent wind-stress data suggest a reasonable degree of realism of the ocean simulation. Also, the annual cycle of the depth of the mixed layer and the spatial heterogeneity of upwelling is compatible with the limited available information from observations.

One conclusion of my study is that in general, no significant long-term trend is detected in the upwelling time series, although this may be due to the short length of the simulation and the small magnitude of the possible long-term trend relative to the interannual variations.

The upwelling intensity and variability are found to be higher along the southern coast than along the northern coast of Oman. This result suggests that upwelling along the southern coast is more intense. In addition, the southern coast is also the region where upwelling is most significantly connected to the ISM but the correlation between them is not as high as expected from previous studies. Therefore, this simulation does not reveal a strong impact of the Indian Monsoon on the western Arabian Sea coastal upwelling.

This low correlation points to other processes that might contribute to the upwelling variability. Both SLP and ST are considered and are compared with the upwelling PC1. The comparisons indicate that the upwelling is strongly affected by the SLP gradient between the Himalayas and the Arabian Sea and is also linked to the ST gradient between northern and central India. These two gradients, however, are also connected to the Monsoon (Feng and Hu 2005; Krishnamurthy

and Ajayamohan 2010) so caution should be taken when distinguishing the sources that influence the upwelling. On one hand, the upwelling is weakly correlated to the ISM but significantly correlated to the SLP and the ST gradients; on the other hand, both of the SLP and the ST gradients are associated with the ISM. The contrast and the consistency of the relationship between upwelling PC1 and IMI in their correlations with SLP and ST indicate that the link between Monsoon and ST and between upwelling and ST display similar spatial structures, whereas in the case of SLP the correlation patterns are quite different. The physical explanation is that the SLP pattern that drives upwelling in the Arabian Sea is statistically linked to a similar temperature pattern over India that also tend to appear with the Monsoon. The physical connections are, however, different. Whereas the SLP pattern related to upwelling advects cold temperatures from the Arabian Sea into India, the Monsoon is linked to lower temperatures there likely due to higher rainfall and cloudiness.

The lack of long-term observational data restricts the validation of the results and the data from satellite ocean-colour observations are heavily blocked during the upwelling season in the Arabian Sea. Methods such as the one described by Banzon et al. (2004) will help to recover the gaps in the satellite data and thus the recovered data might be possible to further inspect the results in this study.

CHAPTER 3

Arabian Sea upwelling over the last millennium as simulated by Earth System Models

3.1 Introduction

Upwelling lifts the cold nutrient-rich water from deeper ocean layers to the surface, which cools the surface water and provides the biologically active layers with nutrients. It has a great impact on human activities. For instance, about 20% of the total marine fish catches originate from upwelling regions that cover only 2% of the entire ocean area (Pauly and Christensen 1995). Upwelling also affects the climate by cooling the sea surface temperature (SST) and by influencing the air-sea interactions associated with the variation of SST (Izumo et al. 2008). It has been suggested that, under the global warming scenario, coastal upwelling at global scale would be intensified as the upwelling favourable wind-stress would be strengthened due to the enhanced air-sea temperature gradient (Bakun 1990). Numerous studies have provided insights into the upwelling variations over the last few decades. Most of these studies focus on the four major Eastern Boundary Upwelling Systems (EBUSs), namely, the California (Schwing and

Mendelssohn 1997), Canary (McGregor et al. 2007), Humboldt (Gutiérrez et al. 2011) and Benguela (Santos et al. 2012) upwelling systems. In support of the Bakun hypothesis, Narayan et al. (2010) found positive trends over the late 20th century in all these four coastal upwelling regions and Sydeman et al. (2014) also reported upwelling intensification in the major EBUSs after synthesizing the results from previous studies.

In addition to the major EBUSs, the Arabian Sea is one of the most productive regions in the world. The upwelling along the Oman coast is mainly driven by the southwest (SW) wind-stress which is induced by the Indian summer Monsoon (ISM). Since the link between the ISM and the upwelling is very pronounced, many studies have used the ISM as an indicator of the upwelling, and vice versa. However, direct observations of upwelling in terms of water mass vertical velocity over a long time period are rare, thus, alternative upwelling proxies such as SST, surface wind-stress and sediment records have been generally applied. An alternative tool to analyse upwelling variability is provided by model simulations.

The knowledge of upwelling evolution in the past is crucial to understand and model the upwelling variations at present and to predict them in the future. A widespread approach to study upwelling in the past is through sediment records where the abundance of *G.bulloides* is stored. *G.bulloides* belongs to the phylum foraminifera and is very sensitive to upwelling variations so it is generally used as an upwelling proxy. Over the last millennium the Arabian Sea upwelling is reported to exhibit a slight decrease until approximately 1600 and an abrupt increase afterwards (Anderson et al. 2002; Feng and Hu 2005; Sinha et al. 2011).

I investigate here the Arabian Sea upwelling variation over the last millennium by analysing model simulations of water vertical velocity and by comparing the model results with the observational sediment records to determine the existence of the long-term trends.

3.2 Model and Data

In this study, I analyse the outputs of two earth system models: the Earth System Model of Max-Planck Institute for Meteorology (MPI-ESM) (Giorgetta et al. 2013) and the Community Earth System Model (CESM) (Hurrell et al. 2013). To analyse the upwelling variabilities over the last millennium, I use the paleo configuration of the MPI-ESM (MPI-ESM-P) and the Last Millennium Ensemble (LME) project (Otto-Bliesner et al. 2016) of the Community Atmosphere Model Version 5 from CESM (CESM-CAM5).

The MPI-ESM-P covers the years from 850 to 1849. It has a horizontal resolution of about 2 degrees for the atmosphere (192×96) and about 1 degree for the ocean (256×220). As for its vertical resolution, there are 47 levels in the atmosphere and 40 levels in the ocean. The CESM-CAM5 covers the same period as the MPI-ESM-P. The horizontal resolution of the CESM-CAM5 for the ocean is about 1 degree on the longitude and 0.5 degree on the latitude (320×384). For the atmosphere, it has a horizontal resolution of 2.5 degrees on the longitude and 1.875 degrees on the latitude (144×96). On the vertical, the CESM-CAM5 has 60 levels in the ocean and 30 levels in the atmosphere.

Within each model, I analyse an ensemble of three simulations which have almost the same external forcings but started with different initial conditions. The differences between simulations within each ensemble provide an estimation of the amplitude of internal climate variability, whereas the signal shared by all simulations will approximately represent the response to the imposed external forcing (Tim et al. 2016).

I investigate several variables that are modelled by the simulations, including upwelling velocity, SST, surface wind-stress, wind speed, and sea level pressure (SLP). The upwelling velocity is the "vertical velocity" in the CESM-CAM5 ensembles but has to be derived from the "vertical water mass transport" for the MPI-ESM-P ensembles. Since upwelling along the western Arabian Sea

coast occurs from 200 meters below the ocean surface (Brock and McClain 1992), I average the upper 200 meters of the data. I use the monthly data from the models and because the upwelling season starts in May and ends in September (Brock et al. 1991), only the summer months June, July and August (JJA) are selected. One exception is that for the SST I choose July, August and September (JAS) due to the lag in the response of SST to the upwelling (Rixen et al. 2000). In addition to the modelled data, I also apply the sediment records used by Anderson et al. (2002) to compare with my results.

3.3 Last millennium Upwelling variability

3.3.1 Mean and long-term variation of Upwelling

The mean summer upwelling velocities in the Arabian Sea modelled by MPI-ESM-P and CESM-CAM5 for the last millennium are presented in Fig. 3.1. To avoid duplication, I only show the results of one simulation from each of these two simulation ensembles since the three simulations in each ensemble share very similar spatial patterns. The models present identical patterns of the summer upwelling in the Arabian Sea where strong upwelling occurs along the coast especially on the western coast, induced by the southwest wind-stress (Fig. 3.1a and 3.1b). Upwelling along the west coast is more intense in the MPI-ESM-P simulation, where the velocity can reach 1.5 m/day, than in CESM-CAM5, where the maximum velocity is around 1 m/day. The magnitude of these velocities is reasonable as it matches the estimated order of magnitude suggested from studies focused on present period (Rixen et al. 2000; Shi et al. 2000). In addition, weak downwelling in the central Arabian Sea is found in both models. Downwelling here results from the convergence zone generated by the wind-stress curl (Thadathil et al. 2008; Bauer et al. 1991). Thus, the spatial distribution of the vertical velocity is consistent with the Ekman pumping effect (Lee et al. 2000).

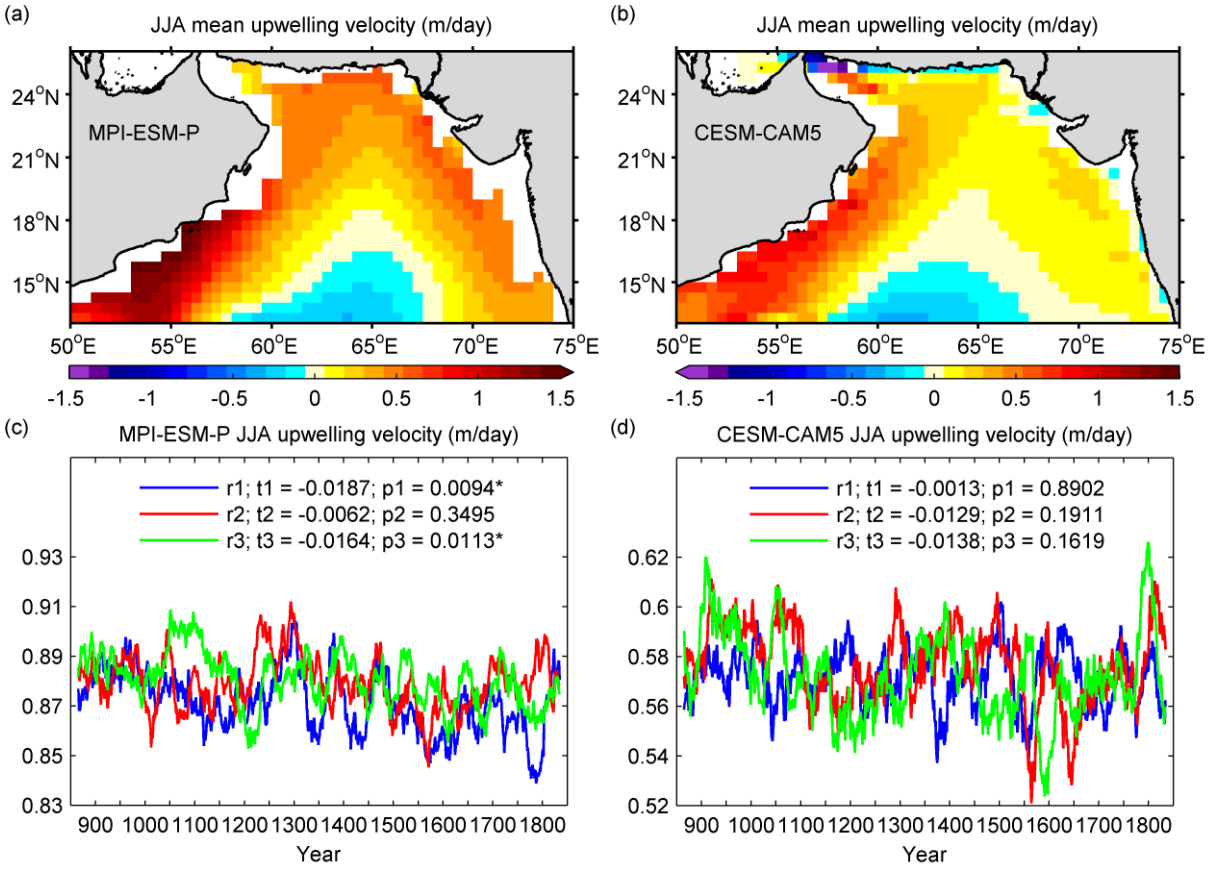

Figure 3.1: Spatial patterns of JJA mean Arabian Sea upwelling velocity modelled by (a) MPI-ESM-P and (b) CESM-CAM5. Time series of JJA upwelling velocity along the west coast of the Arabian Sea modelled by (c) MPI-ESM-P and (d) CESM-CAM5. The plotted time series are smoothed by a 31-year moving mean window and r1, r2, r3 represent the three simulations. t1, t2, t3 are the trends (per 1000 years) of each simulation with p1, p2 and p3 indicating their p-values respectively and the star symbols mark the simulations that pass the significance test at the 95% level.

I average the upwelling along the west coast and calculate the upwelling velocity time series of this area (Fig. 3.1c and 3.1d). In general, these time series show that on average the mean upwelling velocity modelled by MPI-ESM-P is larger than the one simulated by CESM-CAM5 by

around 0.3 m/day. The multidecadal variation is, however, larger in CESM-CAM5. All six simulations by the two models reveal negative trends of the upwelling velocity although not all of them are significant at the 95% significance level. A detailed interpretation of these trends will be presented in Subsection 3.3.4.

3.3.2 Upwelling correlated with SST and sediment record

Since upwelling lifts the cold water from the deeper layers to the ocean surface during the upwelling season, the SST is often anticorrelated with upwelling in the upwelling region. This relationship is well captured in both of the models (Fig. 3.2a and 3.2b). Strong negative correlations are shown along the coastal upwelling regions and even greater ($r<-0.8$) values are found at some locations along the western coast in the CESM-CAM5 model. I also notice the positive correlation areas in the central Arabian Sea where weak downwelling is revealed as shown in Fig. 3.1a and 3.1b. Downwelling is normally associated with convergence zones on the surface and weaker (stronger) downwelling is related to cooler (warmer) surface water in the same region. In terms of vertical velocity as it is in my case, downwelling is represented by the negative values of vertical velocities, thus larger (smaller) velocities indicate weaker (stronger) downwelling. In principle, the SST should be negatively correlated with the vertical velocities in both upwelling and downwelling regions. However, Fig. 3.2a and 3.2b show positive correlations between SST and vertical velocity in the downwelling region of central Arabian Sea. This is likely due to the effect of horizontal advection (Turner et al. 2012; Lévy et al. 2007).

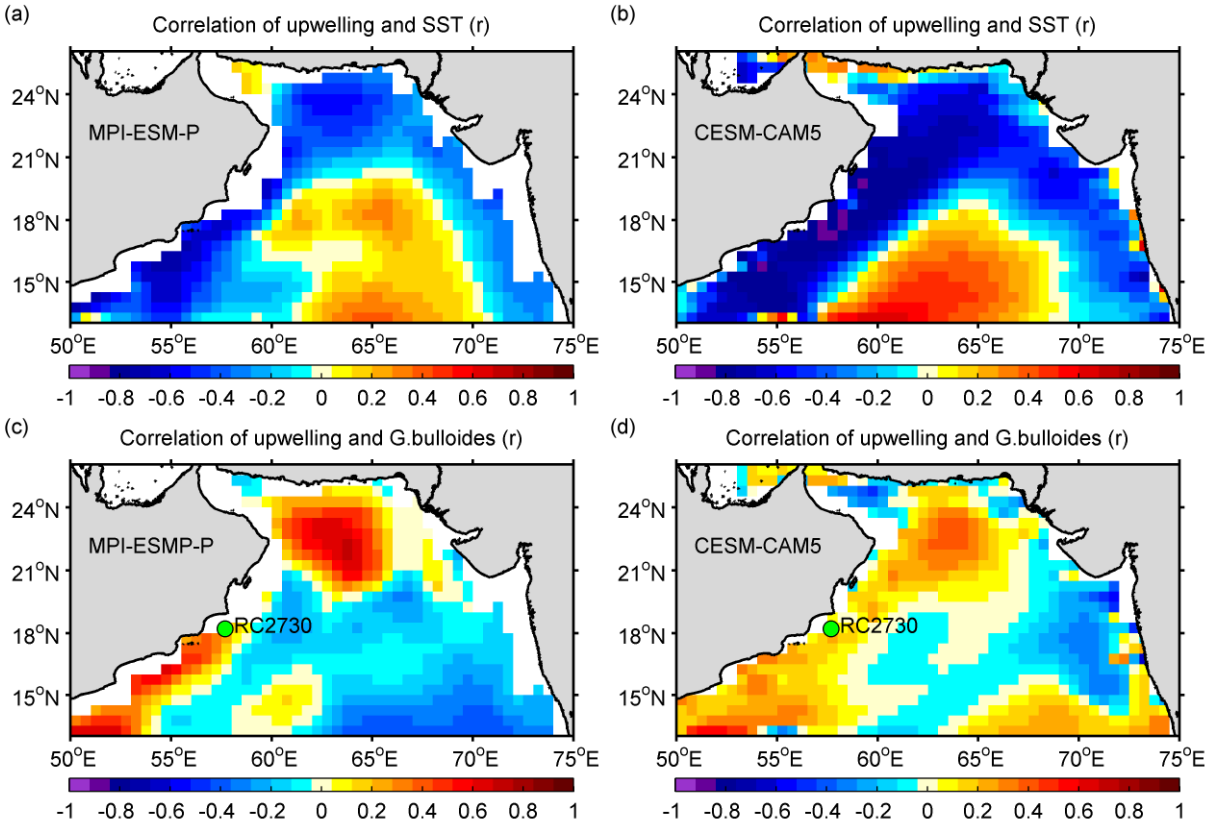

Figure 3.2: Correlation coefficient between the SST and the upwelling velocity modelled by (a) MPI-ESM-P and (b) CESM-CAM5. Correlation coefficient between the *G.bulloides* abundance and the upwelling velocity simulated by (c) MPI-ESM-P and (d) CESM-CAM5. The green point marks the location of the sediment core where the *G.bulloides* abundance is recorded.

On one hand, during the upwelling season strong upwelling occurs along the west coast of the Arabian Sea and the SW wind causes Ekman transport that takes the upwelled cold water from the coast to the centre. On the other hand, the downwelling in the central Arabian Sea is very weak and its influence on the local SST is also very small. Therefore, the cold surface water transported from the coast into the downwelling region dominates the SST variability in the central Arabian Sea and thus the SST is positively correlated with the vertical velocity in the downwelling region.

As a comparison with the sediment records which is considered as the observational data, Fig. 3.2c and 3.2d show the correlations between Arabian Sea upwelling and the *G.bulloides* abundance retrieved from the sediment cores RC2730 and RC2735 (Anderson et al. 2002). This record has been interpreted as an indicator of upwelling in this region (Peeters et al. 2002). I only mark the location of RC2730 on the maps because these two cores are located very close to each other. The calculation of the correlation is performed on the 50-year averaged data during the overlapping years (1050-1849) of the modelled upwelling velocity and the *G.bulloides* abundance. These filtered series presumably reflect the variations in the external forcing, or at least the externally forced component of the variability should be large. Since the external forcing should be ideally the same in the observations and in the simulations, a positive correlation between both records should be expected. However, the records from only two cores located at very close positions might not represent the upwelling in a broader area. In spite of this, the maps present significant correlations along the west coast all the way to the northern Arabian Sea especially for the MPI-ESM-P model. Such correlations indicate that the models reasonably reproduce the variability of upwelling velocities at timescales that are presumably more strongly driven by the external climate forcing than at interannual timescales. The simulated records are thus comparable to the sediment records.

3.3.3 EOF analysis of Upwelling

I perform an Empirical Orthogonal Function (EOF) analysis (von Storch and Zwiers 2001) on the Arabian Sea upwelling to identify its main spatial variation patterns and the corresponding temporal evolutions. EOF analysis can identify the spatial patterns that describe the data variance by generating the EOF modes and their corresponding principal component (PC) time series, where each mode is ranked by its explained proportion of the total variance.

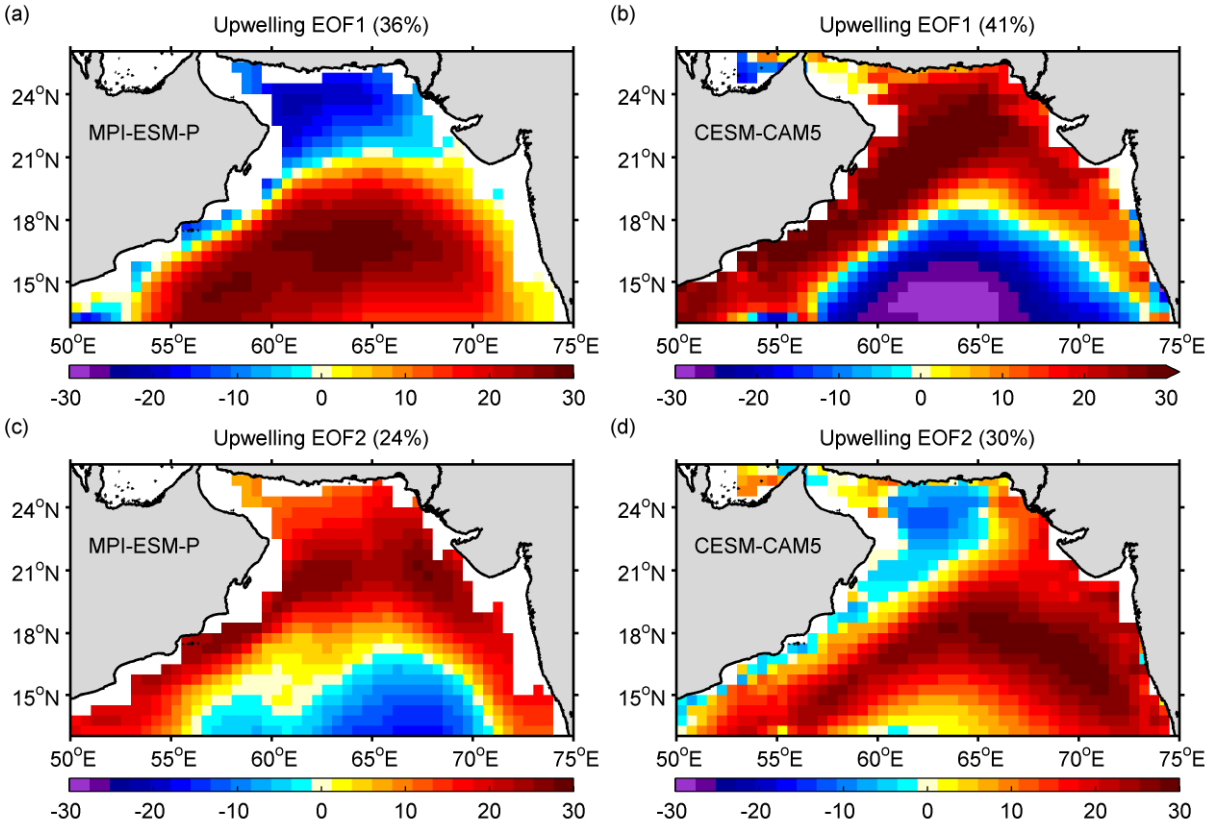

Figure 3.3: First EOF mode of JJA Arabian Sea upwelling velocity modelled by (a) MPI-ESM-P and (b) CESM-CAM5 and second EOF mode from (c) MPI-ESM-P and (d) CESM-CAM5 with their explained variance in brackets.

The leading two modes from the EOF analysis of the upwelling are given in Fig. 3.3. The ranks of the first two modes are switched between MPI-ESM-P and CESM-CAM5. The first mode from CESM-CAM5 (Fig. 3.3b) accounts for 41% of the total variance and reveals similar spatial patterns as the second mode of the MPI-ESM-P simulation (Fig. 3.3c) which accounts for 24% of the total variance. I find that these EOF modes are related to the interannual variations as they capture the spatial patterns of the mean state of the upwelling (Fig. 3.1a and 3.1b) where the different signs between coastal and central Arabian Seas show the contrast between these regions. Their PC time series (Fig. 3.4b and 3.4c) also have a strong positive correlation with the time

series averaged from the western coastal upwelling (Fig. 3.1c and 3.1d) for all the simulations respectively (Tab. 3.1).

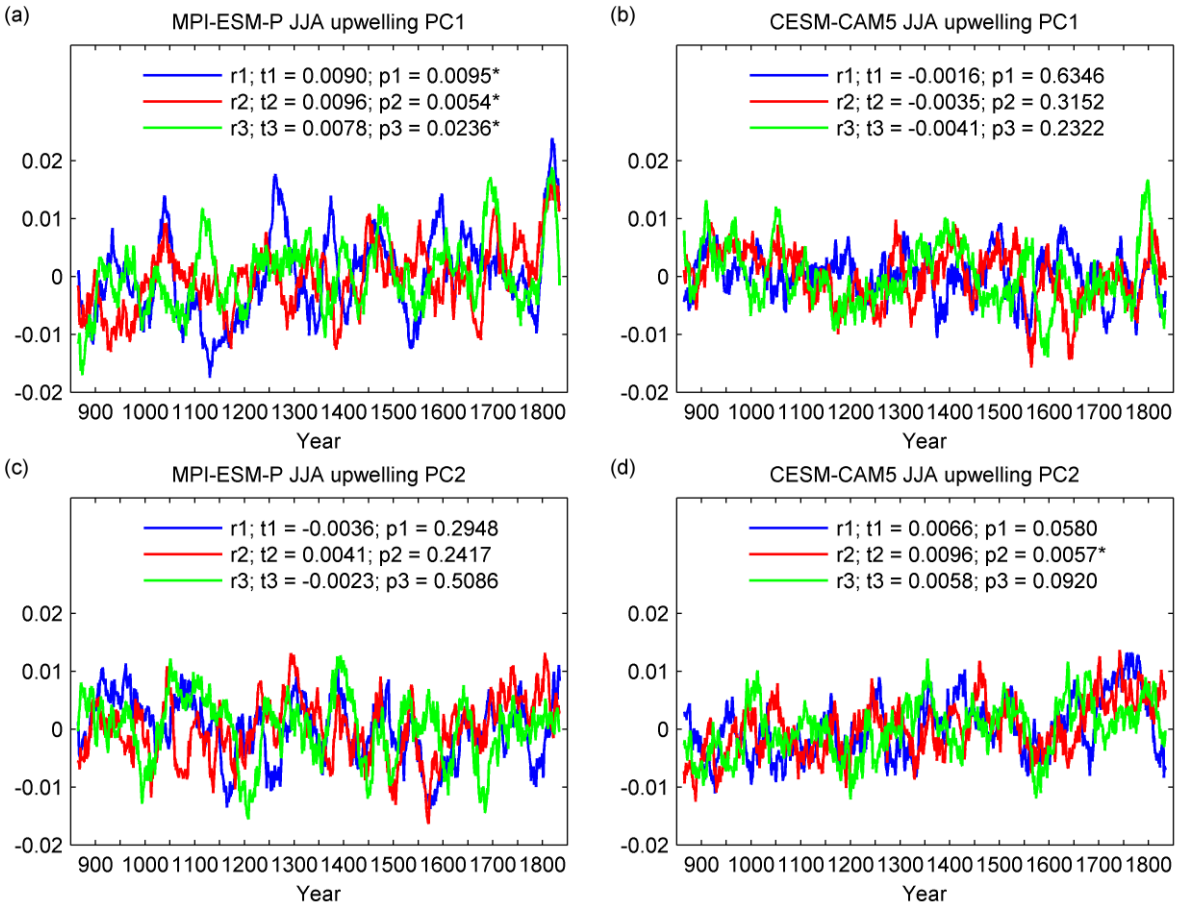

Figure 3.4: First principal component (PC) time series corresponding to the first EOF mode for all the simulation in (a) MPI-ESM-P and (b) CESM-CAM5 and second PC time series of (c) MPI-ESM-P and (d) CESM-CAM5. The plotted PCs are smoothed by a 31-year moving mean window and r1, r2, r3 represent the three simulations. t1, t2, t3 are the trends (per 1000 years) of each simulation with p1, p2 and p3 indicating their p-values respectively and the star symbols mark the simulations that pass the significance test at the 95% level.

Thus, the intensity of the upwelling along the west coast of the Arabian Sea is in phase with the intensity of the upwelling in the rest of the coastal areas and also with the intensity of the

downwelling in the central Arabian Sea. This result is supported by the correlation between upwelling and the Indian Monsoon Index (IMI). I calculate the IMI from the model derived U850 wind data based on the definition of Wang and Fan (1999). The IMI is significantly correlated to the upwelling time series in all the simulations (Tab. 3.1).

Table 3.1: Correlation coefficient between the upwelling velocity along the west coast of the Arabian Sea and the IMI, the upwelling PCs*, and the SLP PC2 for all the six simulations from the two models. (*) Upwelling PC2 is used for correlations within the MPI-ESM-P simulations but upwelling PC1 is used for CESM-CAM5.

	MPI-ESM-P upwelling TS			CESM-CAM5 upwelling TS		
	r1	r2	r3	r1	r2	r3
IMI	0.64	0.61	0.60	0.64	0.66	0.65
Upwelling PCs*	0.79	0.85	0.83	0.92	0.93	0.93
SLP PC2	0.61	0.50	0.55	0.84	0.87	0.83

It is shown in Fig. 3.5a and 3.5b that the IMI is also correlated to the upwelling velocity in the rest coastal areas in the Arabian Sea and the negative correlation in the centre downwelling region indicates that the IMI contributes to the intensification of the downwelling as well. Since the IMI is calculated based on the wind field which is caused by the SLP gradient, I also apply the EOF analysis to the SLP field. I find that the western coastal upwelling time series from both of the models are also significantly correlated with the PC time series of the second mode from the EOF analysis of the SLP (Tab. 3.1).

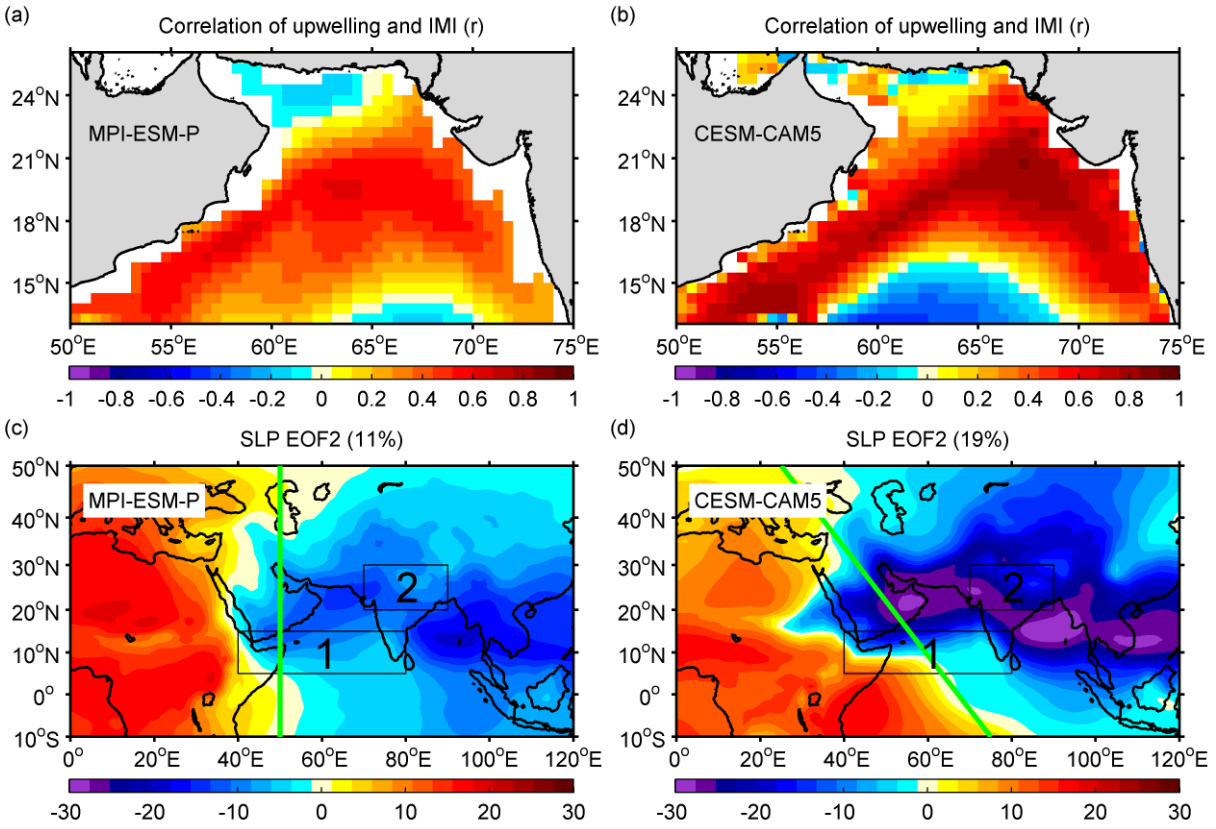

Figure 3.5: Correlation coefficient between the upwelling velocity and the IMI modelled by (a) MPI-ESM-P and (b) CESM-CAM5. The IMI is calculated by subtracting the U850 wind averaged in box2 from that in box1 (boxes shown in c, d). The second EOF mode of JJA SLP modelled by (c) MPI-ESM-P and (d) CESM-CAM5 with their explained variance in brackets. The green lines demonstrate approximately the simplified boundaries that divide the positive and negative EOF phases.

This EOF mode of SLP displays a clear spatial pattern representing the contrast between Africa and Indo-Asia (Fig. 3.5c and 3.5d). In general, the patterns revealed from the two models are very similar. However, the boundary line that separates the positive and negative EOF phases rotates anticlockwise in CESM-CAM5 comparing to that in MPI-ESM-P. This tilt might be responsible for the 8% more variance captured by the second EOF mode of SLP from CESM-CAM5 than

that from MPI-ESM-P as well as the higher correlation between the SLP PC2 and the western coast upwelling time series derived from CESM-CAM5 than that from MPI-ESM-P (Tab. 3.1). An explanation might be that, with this tilt, the second EOF mode revealed from CESM-CAM5 captures a contrast of the spatial patterns in the southern Arabian Sea, which contributes to the variance representing the SW wind-stress that highly correlates with the western coast upwelling time series.

3.3.4 Study of trends

In order to understand the millennial scale variability of the Arabian Sea upwelling, I calculate the long-term linear trends of the vertical velocity. Fig. 3.6a and 3.6b show the upwelling trends derived from the two simulations. Both models reveal negative trends in the northern Arabian Sea and along the west coast where the intense upwelling occurs. On the contrary, the central and eastern Arabian Seas display positive trends. Note that the central Arabian Sea is dominated by downwelling, and so the positive trends in this region actually indicate a weakening of downwelling, whereas in the eastern Arabian Sea the upwelling is slightly strengthened. However, in the western Arabian Sea, the region of my main focus, the upwelling velocity decreased over the last millennium, whereby the MPI-ESM-P model displays a more significant reduction than the CESM-CAM5 model. The upwelling velocity trends share very similar spatial patterns with the first mode of MPI-ESM-P (Fig. 3.3a) and the second mode of CESM-CAM5 (Fig. 3.3d) from the EOF analysis. In addition, their PC time series (Fig. 3.4a and 3.4d) also confirm the trends revealed in the upwelling velocity time series (Fig. 3.1c and 3.1d). The different signs in the EOF spatial patterns and the trends in the PC time series indicate the weakening of the western Arabian Sea coastal upwelling. The trends revealed from the time series are small in terms of their amplitudes over a thousand years compared to the mean upwelling velocity. However, negative trends of western Arabian Sea upwelling are shown consistently in all the six simulations by the two models despite of the different internal conditions used for the simulations. Therefore, the weakening of upwelling in this region is very likely a robust feature in the simulations.

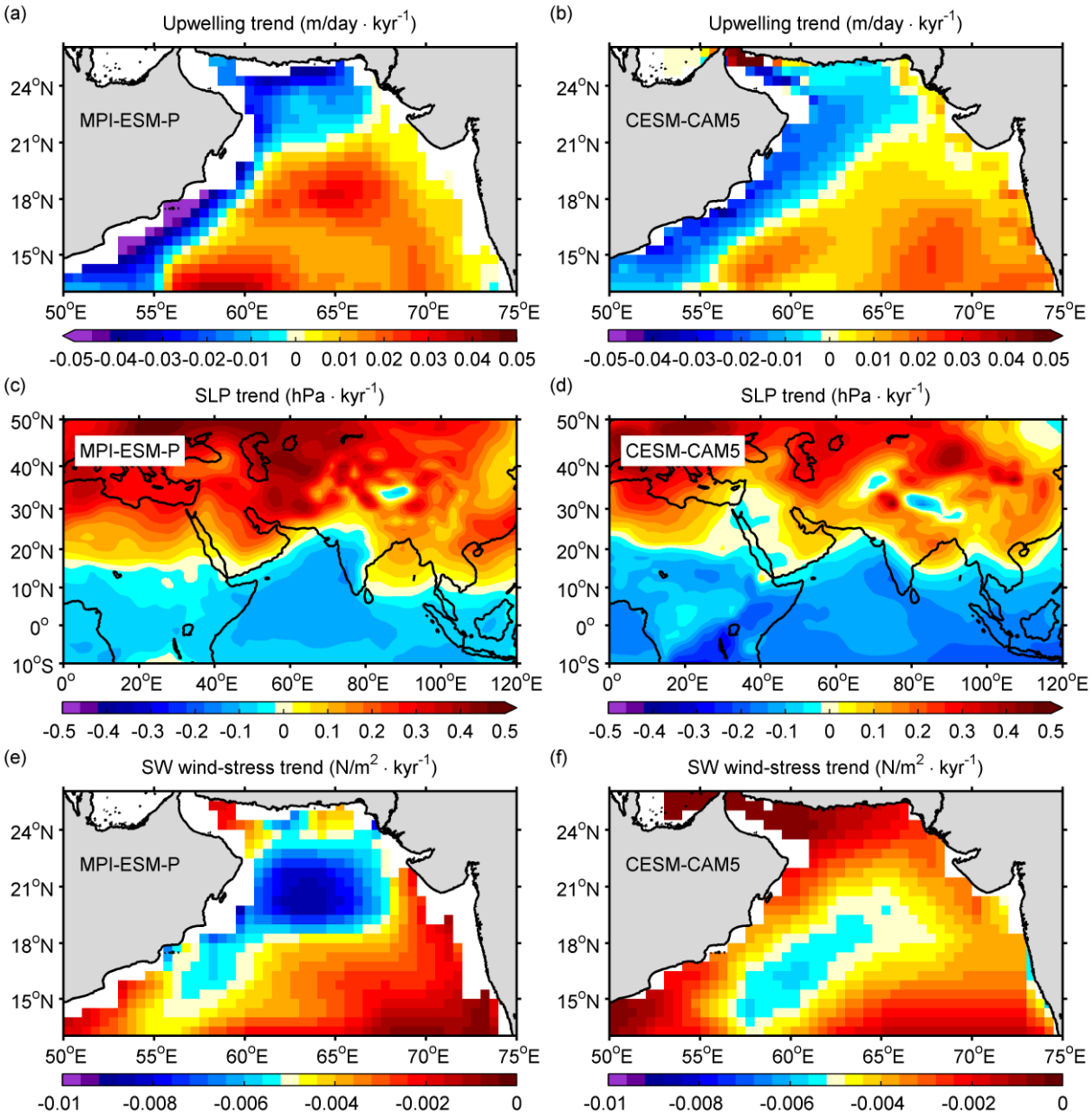

Figure 3.6: Long-term trends of JJA upwelling velocity modelled by (a) MPI-ESM-P and (b) CESM-CAM5. Long-term trends of JJA SLP modelled by (c) MPI-ESM-P and (d) CESM-CAM5. Long-term trends of JJA SW wind-stress in the Arabian Sea modelled by (e) MPI-ESM-P and (f) CESM-CAM5.

These trends are likely induced by the external forcing used to drive the models. Among all the external forcings, only the orbital forcing displays the long-term millennial scale trend, so that the identified upwelling trends can presumably be attributed to the orbital forcing.

To confirm the effect of the orbital forcing, I calculate the trends of the SLP (Fig.6c and 6d) and the SW wind-stress (Fig.6e and 6f) since the upwelling is mainly forced by the SW wind-stress which is linked to the SLP gradient. The spatial patterns of the SLP trends show clearly that in mid latitudes the SLP tends to increase and in low latitudes the SLP tends to decrease. These patterns quite likely result from the effect of orbital forcing, as similar long-term changes are also derived from the differences between equilibrium mid-Holocene and present climate simulations (Braconnot et al. 2002). With positive trends in the mid latitudes and negative trends in the low latitudes, the SLP contrast between these areas is reduced, which further affects the wind in the Arabian Sea. During the summer upwelling season, this SLP contrast drives the SW wind so when the SLP contrast is reduced the SW wind is also weakened. Fig.6e and 6f present the negative trends of SW wind-stress, as expected. In general, the trend from MPI-ESM-P is larger than that from CESM-CAM5. Since the western Arabian Sea coastal upwelling is significantly linked to the SW wind-stress in the Arabian Sea, the negative trends of SW wind-stress can cause the decrease in the upwelling velocity (Fig.6a and 6b). A larger trend of SW wind-stress in the case of the MPI-ESM-P model than in the CESM-CAM5 model also results in stronger trend of upwelling. Therefore, the weakening of upwelling along the west coast of the Arabian Sea is induced by the reduction of the SW wind-stress which results from the long-term change of the SLP contrast between mid and low latitudes due to the orbital forcing.

3.4 Discussion and Conclusions

One limitation of this study is that it relies to a great extent on the realism of the models employed, which makes it very difficult to validate the results as there are no available direct observations on upwelling over the time span. However, I do find a connection between my modelled upwelling velocity and the observational sediment records. They present a significant correlation (Fig. 3.2) which indicates the effect of the external forcing. In addition, they also have similar patterns in the time series in terms of the trends. It can be noticed that the long-term trend revealed from the upwelling time series (Fig. 3.1) tends to flip, especially in the CESM-CAM5 model, at around the year 1550. This flip was reported by Anderson et al. (2002) where they reconstructed the upwelling index (monsoon winds) from the sediment records over the last millennium. They found a slightly negative trend from 1000 to 1500 and a positive trend thereafter, which is very similar to my finding. Thus, I divide the upwelling time series into two periods based on the flip and calculate the trends separately (Tab. 3.2).

Table 3.2: Upwelling trends (m/s per 1000 years) calculated from the two models for different time periods: the entire time period (850-1849), the first 700 years (850-1549), and the last 300 years (1550-1849). The star signs indicate the trends that pass the 95% significance level.

	MPI-ESM-P upwelling trend			CESM-CAM5 upwelling trend		
	r1	r2	r3	r1	r2	r3
850 - 1849	-0.0189*	-0.0062	-0.0164*	-0.0013	-0.0129	-0.0138
850 - 1549	-0.0120	-0.0052	-0.0105	-0.0005	-0.0028	-0.0343*
1550 - 1849	0.0567	0.0862*	0.0062	-0.0100	0.1484*	0.0905

It is very clear that five out of six of the simulations indicate a flip in the long-term trend at around 1550 as the signs of the trends change from negative to positive after this point (except for the CESM-CAM5 r1). Therefore, the models are able to produce realistic upwelling velocity time series that agree with the sediment records, but there are still remaining uncertainties. For instance, the exact time when the trends change signs varies from simulation to simulation, which might be caused by the different initial conditions applied for each simulation.

Model resolution also has an impact on the realism of the results (Small et al. 2015; Ranjha et al. 2016). However, it is still unclear which resolution is required to reasonably model the Arabia Sea coastal upwelling system. In my study, the MPI-ESM-P uses a coarser horizontal resolution (256×220) than the CESM-CAM5 (320×384) and produces the upwelling velocity with larger means but less variability, as well as larger trends. The upwelling velocity simulated by the CESM-CAM5, however, has stronger correlation with the wind and the wind-based IMI. Whether these differences are caused by the different resolutions is uncertain but this comparison might shed light on how the modelled Arabian Sea upwelling response to the change in the model resolutions.

It is concluded that over the last millennium the modelled upwelling velocity has a strong correlation with the SST and the IMI as well as the observed *G.bulloides* abundance. This indicates a close connection among the Arabian Sea upwelling, the Indian summer Monsoon and the sediment records. In addition, a negative long-term trend is found in the upwelling velocity over the last millennium, which results from the orbital forcing of the models. In the last 300 years, however, the upwelling reveals a positive trend, which matches the observations in the sediment records.

CHAPTER 4

Arabian Sea upwelling estimated for the 21st century under different future scenarios

4.1 Introduction

Coastal upwelling at global scale is suggested to be intensified due to strengthened along-shore winds caused by enhanced land-sea thermal gradient under greenhouse warming (Bakun 1990). A recent study used the Coupled Model Intercomparison Project Phase 5 (CMIP5) model outputs to conduct an analysis on the 21st century upwelling under the future scenario of Representative Concentration Pathway (RCP) 8.5 (Wang et al. 2015). They indicated that the upwelling intensity and duration are both increased at high latitudes in most of the major EBUSs except California. However, a study focused on the future upwelling in the Arabian Sea is not yet available.

In this chapter, I investigate the evolution of future upwelling in the Arabian Sea estimated by MPI-ESM-LR and CCSM, the same models used in the previous chapter with slightly different configurations for past and future. An ensemble of three simulations with same external forcings

but different initial conditions for each model is selected. I compare the future upwelling under the RCP8.5 and RCP2.6 scenarios to gain the information on how the greenhouse gas emission level could affect the changes in upwelling.

4.2 Trends in the future Upwelling

4.2.1 Scenarios RCP8.5 and RCP2.6

The time series of the upwelling velocity, together with those of the SST and the SW wind-stress simulated by MPI-ESM-LR and CCSM under the scenario RCP8.5 are presented in Fig. 4.1. All the simulations by the two models with the RCP8.5 scenario are quite consistent by showing positive trends in SST and SW wind-stress but negative trends in upwelling velocity. The SST (Fig. 4.1a and 4.1b) increases significantly under the effect of the greenhouse gas emission. In the MPI-ESM-LR model (Fig. 4.1a) the SST begins with lower values than that in the CCSM model (Fig. 4.1b) but they rise to similar values in the end of the simulations so the SST modelled by the MPI-ESM-LR has a lager trend than by the CCSM. The SW wind-stress (Fig. 4.1c and 4.1d) is also strengthened due to the enhanced contrast between the surface heating over the land and the sea. Although all the simulations by both models show positive trends, the CCSM simulations (Fig. 4.1d) reveal more distinct and significant trends than the MPI-ESM-LR (Fig. 4.1c). As a result of the intensification of the wind-stress the upwelling velocity is expected to increase as well. However, negative trends of upwelling velocity are found in all the simulations (Fig. 4.1e and 4.1f) especially for the MPI-ESM-LR (Fig. 4.1e). This raises an interesting question as to what is causing the negative trend in upwelling velocity given that the upwelling favourable wind-stress is projected to increase.

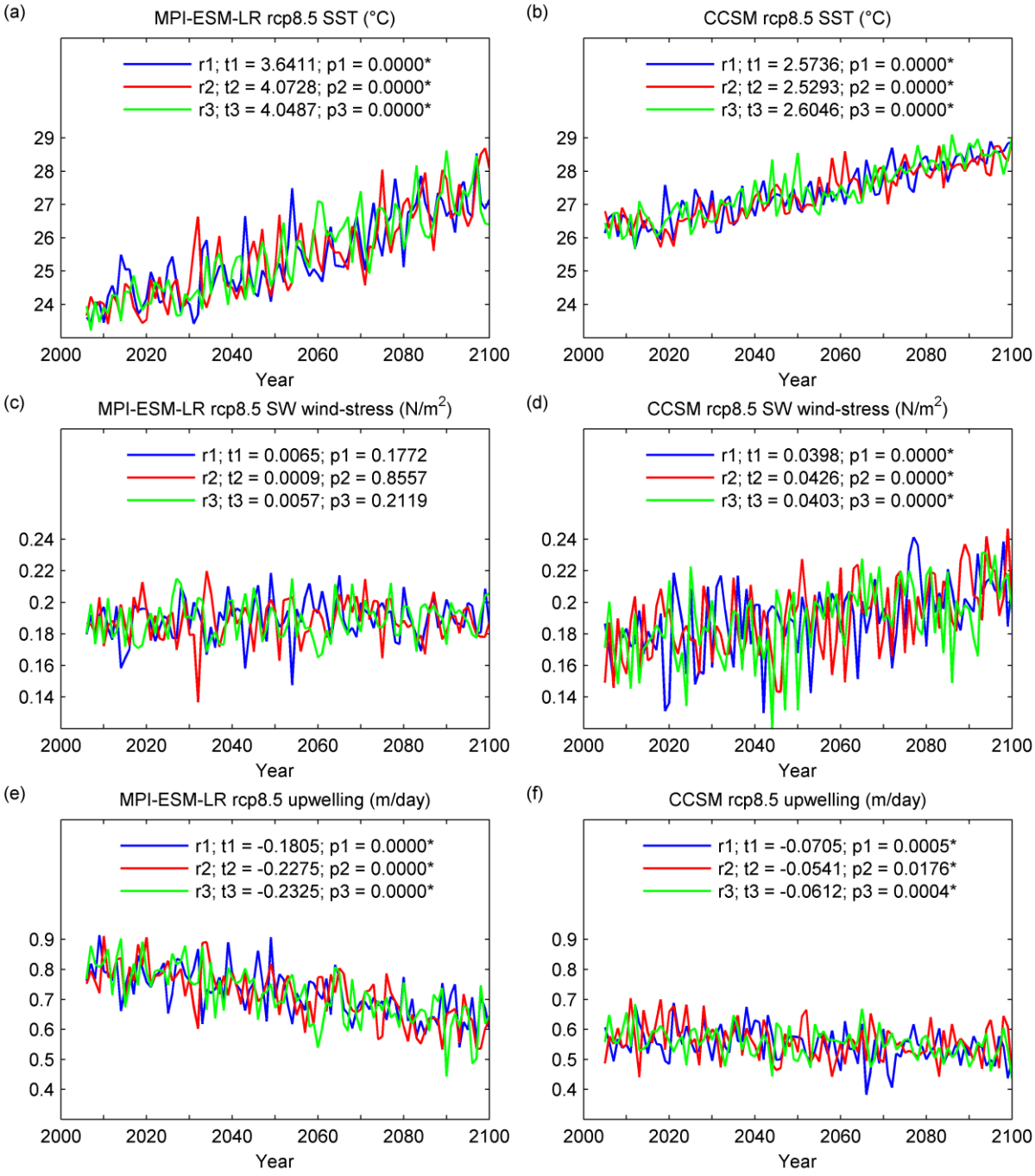

Figure 4.1: Time series of (a) SST, (c) SW wind-stress and (e) upwelling velocity modelled by MPI-ESM-LR under the scenario of RCP8.5 for the 21st century. (b), (d) and (f) are the same variables respectively modelled by CCSM. r1, r2, r3 represent the three simulations of each model.

t1, t2, t3 are the trends (per 100 years) of each simulation with p1, p2 and p3 indicating their p-values respectively and the star symbols mark the simulations that pass the significance test at the 95% level.

Fig. 4.1 shows that the MPI-ESM-LR simulations reveal larger positive trends in SST and at the same time larger trends in upwelling than the CCSM simulations, which implies that the drop in upwelling velocity might be linked to the warming of the upper ocean layers in the RCP8.5 scenario and thus to an increase in stratification. To test this hypothesis, I perform the same analysis for the RCP2.6 scenario (Fig. 4.2). Under the RCP2.6 scenario the SST still increases in both models (Fig. 4.2a and 4.2b) but not as much as in the RCP8.5 scenario. However, no consistent trends for all the simulations are found in the SW wind-stress (Fig. 4.2c and 4.2d) or the upwelling velocity (Fig. 4.2e and 4.2f). Thus, it is very likely that the lack of negative trends in upwelling velocity under scenario RCP2.6 is caused by the negligible ocean surface warming. Note that the correlation between upwelling and SW wind-stress at interannual timescales does not change much in different scenarios (Tab. 4.1), which indicates that the influence of the wind-stress on the upwelling remains at the same level in the two scenarios.

Table 4.1: Correlation coefficient between the upwelling velocity and the SW wind-stress modelled by MPI-ESM-LR and CCSM for the RCP8.5 and RCP2.6 scenarios. All the correlation coefficients are calculated from the detrended time series and are significant at the 95% significance level.

	MPI-ESM-LR			CCSM		
	r1	r2	r3	r1	r2	r3
RCP8.5	0.5457	0.4787	0.5420	0.4844	0.5500	0.5321
RCP2.6	0.4270	0.4259	0.4752	0.7569	0.6391	0.6879

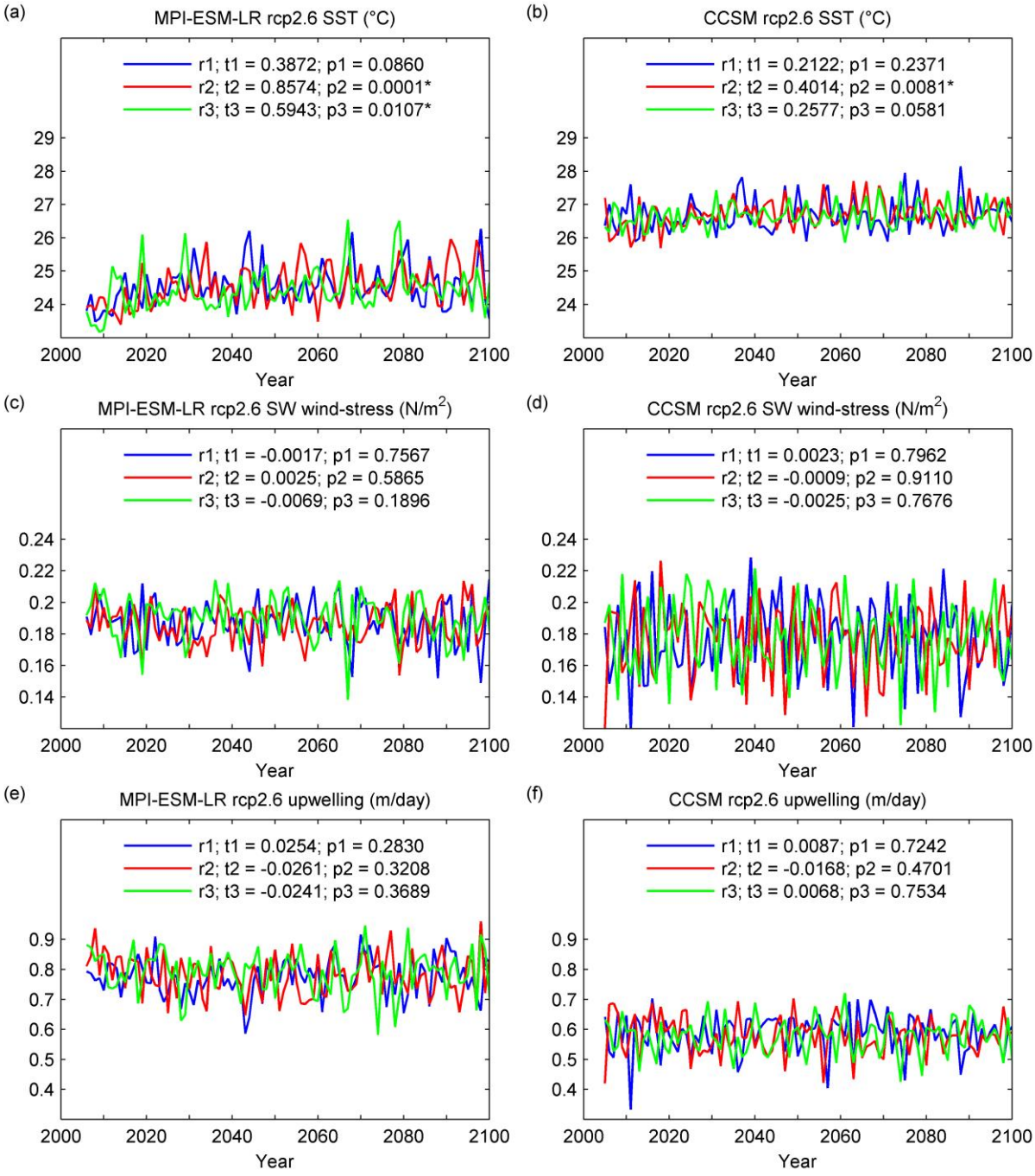

Figure 4.2: Time series of (a) SST, (c) SW wind-stress and (e) upwelling velocity modelled by MPI-ESM-LR under the scenario of RCP2.6 for the 21st century. (b), (d) and (f) are the same variables respectively modelled by CCSM. r1, r2, r3 represent the three simulations of each model.

t1, t2, t3 are the trends (per 100 years) of each simulation with p1, p2 and p3 indicating their p-values respectively and the star symbols mark the simulations that pass the significance test at the 95% level.

The correlation between upwelling and the SW wind-stress is slightly weaker in the RCP2.6 than in the RCP8.5 scenarios from the results of the MPI-ESM-LR but stronger from the CCSM. However, the significant positive correlation between upwelling velocity and the SW wind-stress does not lead the evolutions of upwelling and wind-stress towards the same direction under a stronger greenhouse gas emission scenario (Fig. 4.1). One explanation for this is that even though the correlation between upwelling and the SW wind-stress remains at the same level in the two scenarios, the significant rise in the SST under the RCP8.5 scenario might override the effect of the wind-stress. Although wind-stress still drives upwelling, its effect is obstructed by the more stable water column due to surface warming effect.

4.2.2 Vertical trends

To confirm the effect of the water stratification on the upwelling velocity, I examine the vertical trends and means of water temperature and upwelling velocity modelled by the two models for the RCP2.6 and the RCP8.5 scenarios. The differences in the trends at all levels in the upper 200m between the RCP8.5 and RCP2.6 scenarios are shown in Fig. 4.3. There are slight positive trends for RCP2.6 and significant trends for RCP8.5 in the water temperature (Fig. 4.3a and 4.3c). There are also no consistent trends in the upwelling for RCP2.6 but significant negative trends at all levels for RCP8.5 (Fig. 4.3b and 4.3d). In the upper 50m to 100m the upwelling velocity show larger negative trends when the trends of the water temperature increase, which is very clearly shown in the CCSM plots (Fig. 4.3c and 4.3d). At around 50m depth the temperature trends reach their peaks and the upwelling trends also get to their lowest values (in the surface layer above 100m). The upwelling is actually most intense at this layer (Fig. 4.3d) but it is most reduced

as well, which causes the drop in the upwelling time series shown in Fig. 4.1. Therefore, in spite of the positive correlation between the SW wind-stress and the upwelling, the warming of the upper ocean layers under the RCP8.5 scenario reduces the upwelling velocity more efficiently.

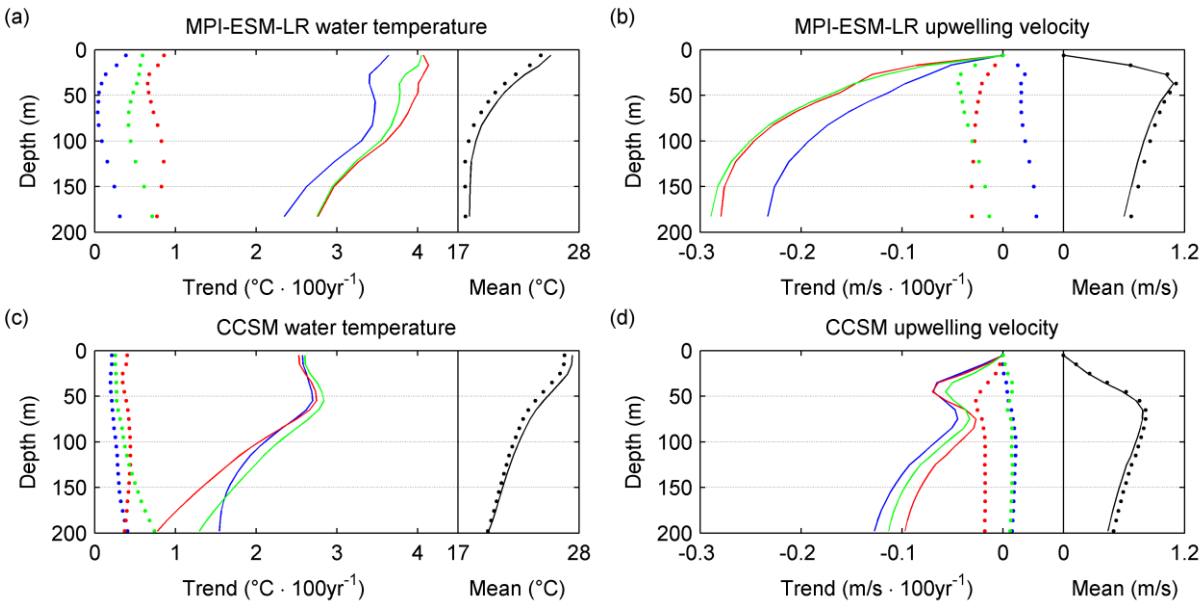

Figure 4.3: Vertical trends of (a) water temperature and (b) upwelling velocity in the upper 200m modelled by MPI-ESM-LR. (c) and (d) are the same but by CCSM. Solid lines are the results for the RCP8.5 scenario and dotted lines are for the RCP2.6 scenario. The coloured lines show the trends of r1 (blue), r2 (red), and r3 (green) in each model. The black lines on the right of each panel present the mean value of the current variable.

4.3 Link with the Indian summer Monsoon

Similar to the previous analyses, I calculate the Indian Monsoon index (IMI) based on the U850 wind derived by the two models. The long-term variation of the IMI derived by all the simulations is shown in Fig. 4.4.

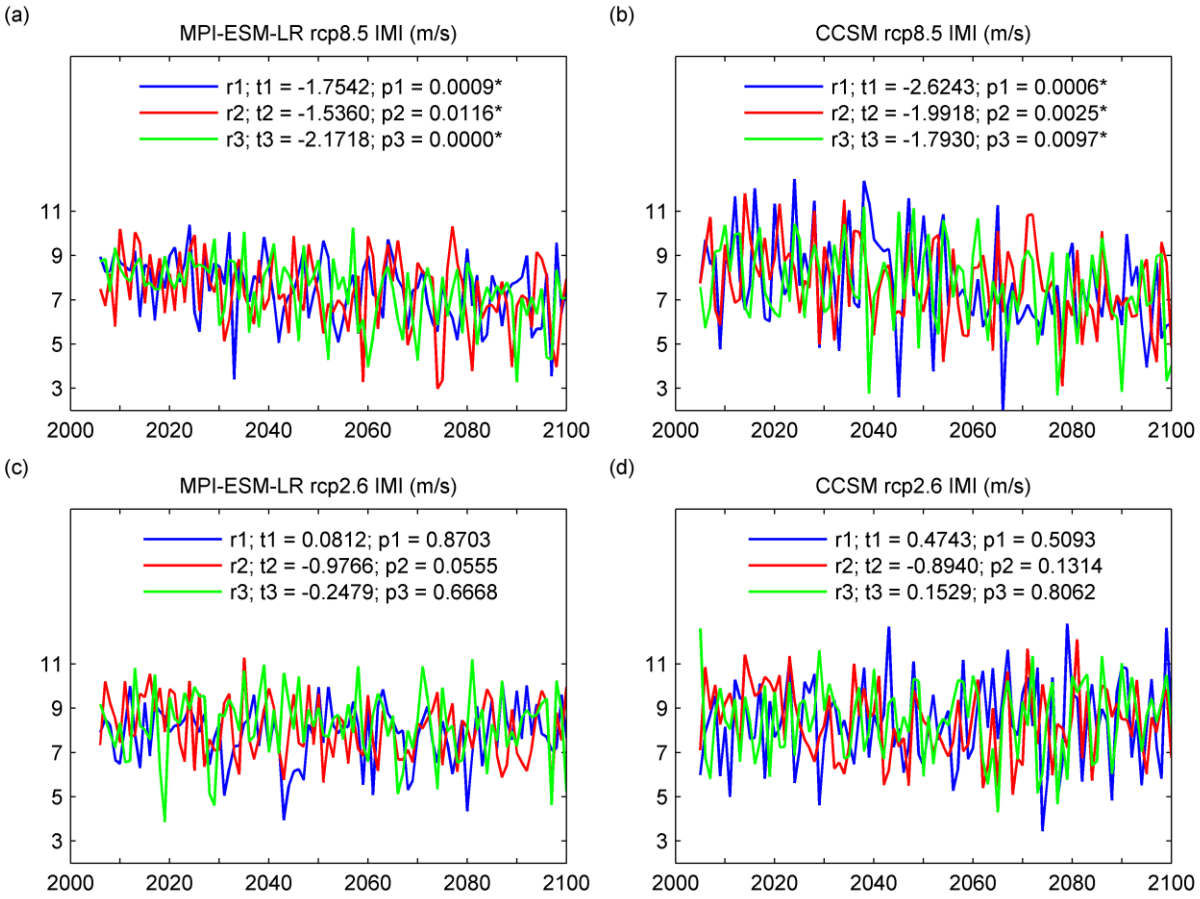

Figure 4.4: Time series of IMI modelled by (a) MPI-ESM-LR and (b) CCSM under the scenario of RCP8.5 for the 21st century. (c) and (d) are the same but for the RCP2.6 scenario. r1, r2, r3 represent the three simulations of each model. t1, t2, t3 are the trends (per 100 years) of each simulation with p1, p2 and p3 indicating their p-values respectively and the star symbols mark the simulations that pass the significance test at the 95% level.

Significant negative trends are revealed from all the simulations for the RCP8.5 scenario, however, no consistent trend is found in the RCP2.6 scenario. This result is related to the estimated upwelling time series, which also show negative trends in the RCP8.5 scenario but no trends in the RCP2.6 scenario. In addition, the IMI and upwelling present strong correlations in both scenarios (Fig. 4.5).

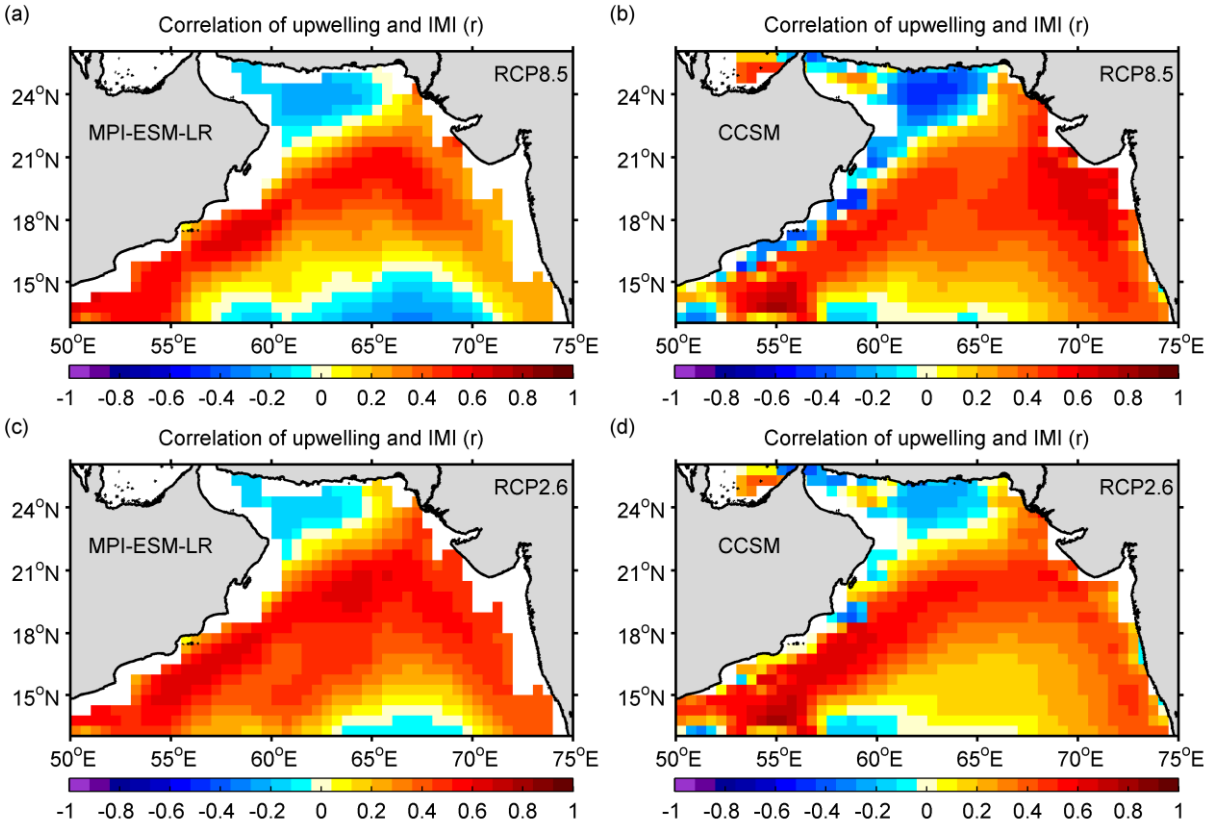

Figure 4.5: Correlation coefficient between the upwelling velocity and the IMI modelled by (a) MPI-ESM-LP and (b) CCSM under the future scenario of RCP8.5. (c) and (d) are the same but for the RCP2.6 scenario.

The patterns of the correlations show clear similarities between the models and between the scenarios. In addition, they are also very similar to the correlation patterns between the upwelling and the IMI revealed from the last millennium analysis (Fig. 3.5). Therefore, the correlation between the IMI and the upwelling is profound in the last millennium simulations and in the future estimations but rather non-significant in the STORM simulation.

4.4 Discussion and Conclusions

In my analysis for the future scenario RCP8.5, the upwelling velocity reveals a negative trend, which matches the finding of a recent study that a reduction in the future upwelling is shown at low latitudes in most of the four EBUSs (Wang et al. 2015). However, the modelled simulated SW wind-stress presents a positive trend, thus, the reduction of the upwelling is not caused by the wind-stress, although they are still significantly correlated. The analysis for the RCP2.6 scenario does not show a trend in either the upwelling or the SW wind-stress but it shows strong correlation between upwelling and the wind-stress as well as the RCP8.5 scenario. Wang et al. (2015) suggested several mechanisms that could lead to a reduction in the upwelling at low latitudes such as strengthened downwelling favourable winds, weakened upwelling favourable winds, and enhanced water stratification due to the greenhouse warming. In my case, it is the more strongly stratified water column that reduces the upwelling under the RCP8.5 scenario, but this is not shown in the RCP2.6 scenario. Therefore, it remains for further study to investigate at what level of future emissions, between the strongest and the weakest warming scenarios, water stratification and the effect of wind-stress approximately balance.

To conclude, I found that the correlation between upwelling and the SW wind-stress remains at the same level under the RCP8.5 and RCP2.6 scenarios in the future but the stronger greenhouse gas emission scenario leads to opposite trends in the SW wind-stress and the upwelling velocity. The positive trend in the SW wind-stress is caused by the intensified SLP gradient between land and ocean due to the warming effect. The upwelling velocity shows a negative trend because under the stronger scenario, the warming of the sea water tends to stabilize the surface layer, which overrides the effect of the SW wind-stress and hinders the upwelling.

CHAPTER 5
Summary and Outlook

5.1 Summary

This thesis focuses on the coastal upwelling in the western Arabian Sea, one of the most important upwelling systems. The primary goal is to examine the impact of large-scale climate patterns on the upwelling variability. I statistically analysed several model simulations and compared them with reanalysis and observational data. The study is divided into three parts based on a chronological scheme: the present, the past and the future. The main results of each part are summarized in this section.

5.1.1 The present

Arabian Sea upwelling in the present (1950-2010) is simulated by the high-resolution ocean-only simulation STORM (10km). The modelled vertical velocity reveals a seasonal signal indicating that the upwelling starts in May and ends in September with a peak in July. In summer, the mean vertical velocity along the western coast of the Arabian Sea is about 1.8 m/day and around the

cape areas the velocity can excess 6 m/day. In general, the upwelling intensity and variability are higher in the south than in the north of the Arabian Sea. The EOF analysis shows clear patterns between coastal and off-shore areas. However, the leading EOF mode accounts for only 10% of the total variance, which implies that the spatial distribution of upwelling in this region is very heterogeneous and the upwelling is affected by complex processes in addition to the large-scale wind forcing. No significant long-term trend is detected for the study period but decadal variability is presented. From 1960 to 1985, the signs of the 15-year and 20-year trends change from negative to positive whereas the 10-year trend experiences a 10-year cycle during this period. Three indices of the Indian Monsoon are employed to examine the relationship between the Monsoon and the upwelling. However, none of the indices show the expected high correlations with upwelling. Higher correlation coefficients are found along the southern part of the coast yet they are still lower than 0.5. This is a quite surprising result since previous understanding indicated that the Arabian Sea upwelling is very closely linked to the Indian summer Monsoon.

I study the mechanism behind this result by analysing the sea level pressure (SLP) and surface air temperature (ST) fields. The upwelling PC1 positively correlates with the SLP over the Arabian Sea and negatively over the Asia continent but the Indian Monsoon Index (IMI) shows an opposite correlation pattern. This might explain the strong correlation between the upwelling and the southwest wind-stress and the low correlation between upwelling and the IMI. The comparison between the upwelling PC1 and the IMI in the ST field shows significantly negative correlations in the Arabian Sea for the upwelling PC1 and over the Indian subcontinent for the IMI. The correlation between the IMI and the ST over India is due to the monsoonal rainfall and the correlation between the upwelling PC1 and the ST over the Arabian Sea is related to the impact of the southwest winds on the upwelling. Thus, it is concluded that although the upwelling and the Monsoon both cause a decrease in the temperature, the mechanisms are different.

5.1.2 The past

Two earth system models (MPI-SEM-P and CESM) are used to study the Arabian Sea upwelling in the last millennium (850-1849). For each model, an ensemble of three simulations with same external forcing but different initial conditions is investigated. In general, all the simulations show very similar results. The mean upwelling velocity over the last millennium is about 50% lower than that simulated for the last 61 years (the present) but still reasonable considering the coarser resolution of the last millennium models compared to STORM and the broader coastal area selected for calculation of the upwelling time series.

The consistency of the upwelling long-term trends revealed from the simulations indicates that the trends are very likely caused by external forcing. The upwelling is strongly correlated with the SST and the IMI (in contrast to the STORM simulation). In addition, I find significant correlation between the upwelling and the *G.bulloides* abundance collected from the sediment records. This also reflects the effect of the external forcing since the external forcing is likely similar in the observations and the models. The modelled trend in SLP shows a very similar spatial pattern to the SLP change between derived from equilibrium mid-Holocene and present simulations. This supports the role of the orbital forcing, the only external forcing that displays the long-term millennial scale trend. Therefore, the negative long-term trend of the upwelling is resulting from the reduced SLP contrast induced by the orbital forcing of the models. In addition to the negative millennial trend, the trend in the upwelling time series reveal a flip in the last 300 years, which matches the sediment records, suggesting that the recent increase in radiative forcing over the last centuries may have caused this flip.

In spite of the many similarities between the results simulated by the MPI-ESM-P and the CESM models, one minor difference is shown in the EOF analysis of the upwelling. The ranks of the leading two EOF modes are switched in the two models. These two modes together contribute 60% and 71% of variance of the upwelling modelled by MPI-ESM-P and CESM, respectively.

This switch is likely caused by the difference revealed in the second EOF modes of SLP between the two models.

5.1.3 The future

I use the same models as used for the last millennium study, but with slightly different configurations (MPI-ESM-LR and CCSM), to examine the projections of Arabian Sea upwelling in the 21st century. Like the previous analysis, an ensemble of three simulations of each model is applied. The results simulated under the strongest (RCP8.5) and the weakest (RCP2.6) greenhouse gas emission scenarios are compared.

Both models present consistent results, showing that under the RCP8.5 scenario the future upwelling is reduced, whereas the SW wind-stress displays positive trends. In addition, the upwelling and the SW wind-stress are significantly correlated at interannual timescales, with positive coefficients in both scenarios. Therefore, in the future scenarios the SW wind-stress is responsible for the interannual variability of the upwelling but not for the long-term change. It is quite likely that the greenhouse warming effect leads to the reduction of upwelling in the RCP8.5 scenario due to the strong warming at the ocean surface which increases the stratification and the stability of the water column.

In the RCP2.6 scenario neither the upwelling nor the SW wind-stress shows consistent trends. I interpret this lack of trend as an approximate balance between the increase in upwelling favourable wind-stress and the increased stratification in this scenario.

To ascertain this explanation, and determine how the warming might influence the upwelling, I calculate the vertical profiles of the upwelling and the sea water temperature in the upper 200 meters along the western Arabian Sea coast. The result presents homogeneous long-term changes of upwelling and water temperature through all levels under the RCP2.6 scenario. However, in

the RCP8.5 scenario the water temperature displays the strongest trends at about 50 meters below surface, where the mean upwelling velocity peaks. Moreover, the CCSM upwelling trends profile shows that the upwelling is also significantly weakened at this level. In conclusion, under the RCP8.5 scenario the upwelling is reduced due to the stratification of the upper water caused by strong greenhouse warming effect.

5.2 Outlook

This thesis provides insights into the future work on the Arabian Sea upwelling. It has to be underlined that the presented results rely to a great extent on the realism of the models used here. The models employed here have been globally tested and validated, but in my case the availability of observations of the Arabian Sea upwelling in terms of vertical velocity is rather limited. Thus, it is very difficult to completely validate the model derived upwelling velocity in this region. Besides, the model resolution might also affect the results. For instance, strong correlation between the upwelling and the IMI is revealed in the past and the future simulations modelled by the MPI-ESM with a resolution of 1° but a relatively low correlation is presented in the present simulation of STORM (0.1°). Although there could be many reasons for this difference, the resolution of the models could be one of them. Recent studies focused on the Benguela upwelling system have discussed the sensitivity of upwelling to the model resolutions (Small et al. 2015; Desbiolles et al. 2016) yet such issue remains unknown in the Arabian Sea. Therefore, in the future work regarding the Arabian Sea upwelling, it will be essential to systematically analyse the difference in upwelling simulated by models of different spatial resolutions, and compare them with available observations.

Another remark is on the upwelling long-term trends revealed from this thesis. According to Bakun (1990), coastal upwelling at global scale, mostly at the EBUSs, would be intensified due to the strengthened thermal gradient between land and sea caused by the effect of global warming.

Many studies have supported the Bakun hypothesis, whereas some other works have shown that this hypothesis depends on the region, the time period and the database used for the study. In my case the Arabian Sea upwelling does not exhibit a long-term trend for the last 61 year or for the 21st century under the RCP2.6 scenario and neither does the SW wind-stress. In the last millennium simulations both the upwelling and the SW wind-stress present negative long-term trends caused by the orbital forcing of the models. However, in the RCP8.5 scenario the upwelling decreases whereas the SW wind-stress increases. I have tried to explain the possible mechanisms that affect the connection between the upwelling and the SW wind-stress during different time periods. The next step of the work would be conducted by including the analyses of the historical simulations from 1850 to 2005 as well as a moderate warming scenario of RCP4.5 for the future. The long-term variation of the upwelling will then be studied through a complete time series from 850 to 2100.

Abbreviations

AVHRR	Advanced Very High Resolution Radiometer
CCMP	Cross-Calibrated Multi-Platform
CESM	Community Earth System Model
CESM-CAM5	Community Atmosphere Model Version 5 from CESM
CliSAP	Cluster of Excellence "Integrated Climate System Analysis and Prediction"
DFG	German Research Foundation
EBUSs	Eastern Boundary Upwelling Systems
EOF	Empirical Orthogonal Function
IITM	Indian Institute of Tropical Meteorology
IMI	Indian Monsoon Index
IMR	All India Monsoon Rainfall index
ISM	Indian Summer Monsoon
JAS	July-August-September
JJA	Jun-July-August
JJAS	June-July-August-September
MLD	Mixed Layer Depth
MPI-ESM	Earth System Model of Max Planck Institute for Meteorology
MPI-ESM-LR	MPI-ESM on Low Resolution
MPI-ESM-P	MPI-ESM on low resolution and Paleo mode
MPI-OM	Max-Planck Institute Ocean Model
NCAR	National Center for Atmospheric Research

NCEP	National Center for Environmental Prediction
PC	Principal Component
RCP	Representative Concentration Pathway
SeaWiFS	Sea-Viewing Wide Field-of-View Sensor
SLP	Sea Level Pressure
SST	Sea Surface Temperature
ST	Surface air Temperature
STD	Standard Deviation
SW	Southwest
U850	Zonal wind speed at 850 hPa
WYM	Webster and Yang Monsoon index

Bibliography

Anderson DM, Brock JC, Prell WL (1992) Physical upwelling processes, upper ocean environment and the sediment record of the southwest monsoon. Geol Soc Sp 64:121-129 doi:10.1144/gsl.sp.1992.064.01.08

Anderson DM, Prell WL (1993) A 300 KYR Record of Upwelling Off Oman during the Late Quaternary: Evidence of the Asian Southwest Monsoon. Paleoceanography 8:193-208 doi:10.1029/93PA00256

Anderson DM, Overpeck JT, Gupta AK (2002) Increase in the Asian Southwest Monsoon During the Past Four Centuries. Science 297:596-599 doi:10.1126/science.1072881

Anderson DM, Baulcomb CK, Duvivier AK, Gupta AK (2010) Indian summer monsoon during the last two millennia. Journal of Quaternary Science 25:911-917 doi:10.1002/jqs.1369

Atlas R, Hoffman RN, Ardizzone J, Leidner SM, Jusem JC, Smith DK, Gombos D (2011) A Cross-calibrated, Multiplatform Ocean Surface Wind Velocity Product for Meteorological and Oceanographic Applications. B Am Meteorol Soc 92:157-174 doi:10.1175/2010BAMS2946.1

Bakun A (1973) Coastal upwelling indices, west coast of North America, 1946-71. NOAA Technical Report NMFS SSRF-671

Bakun A (1990) Global Climate Change and Intensification of Coastal Ocean Upwelling. Science 247:198-201 doi:10.1126/science.247.4939.198

Bakun A, Nelson CS (1991) The Seasonal Cycle of Wind-Stress Curl in Subtropical Eastern Boundary Current Regions. J Phys Oceanogr 21:1815-1834 doi:10.1175/1520-0485(1991)021<1815:TSCOWS>2.0.CO;2

Banse K (1959) On upwelling and bottom-trawling off the southwest coast of India. Journal of the Marine Biological Association of India 1:33-49

Banse K, English DC (2000) Geographical differences in seasonality of CZCS-derived phytoplankton pigment in the Arabian Sea for 1978–1986. Deep Sea Res Part II 47:1623-1677 doi:10.1016/S0967-0645(99)00157-5

Banzon VF, Evans RE, Gordon HR, Chomko RM (2004) SeaWiFS observations of the Arabian Sea southwest monsoon bloom for the year 2000. Deep Sea Res Part II 51:189-208 doi:10.1016/j.dsr2.2003.10.004

Bauer S, Hitchcock GL, Olson DB (1991) Influence of monsoonally-forced Ekman dynamics upon surface layer depth and plankton biomass distribution in the Arabian Sea. Deep Sea Research Part A Oceanographic Research Papers 38:531-553 doi:10.1016/0198-0149(91)90062-K

Braconnot P, Loutre M, Dong B, Joussaume S, Valdes P (2002) How the simulated change in monsoon at 6 ka BP is related to the simulation of the modern climate: results from the Paleoclimate Modeling Intercomparison Project. Climate Dynamics 19:107-121 doi:10.1007/s00382-001-0217-5

Brock JC, McClain CR, Luther ME, Hay WW (1991) The phytoplankton bloom in the northwestern Arabian Sea during the southwest monsoon of 1979. J Geophys Res Oceans 96:20623-20642 doi:10.1029/91JC01711

Brock JC, McClain CR (1992) Interannual variability in phytoplankton blooms observed in the northwestern Arabian Sea during the southwest monsoon. J Geophys Res Oceans 97:733-750 doi:10.1029/91JC02225

Brock JC, McClain CR, Anderson DM, Prell WL, Hay WW (1992) Southwest Monsoon Circulation and Environments of Recent Planktonic Foraminifera in the Northwestern Arabian Sea. Paleoceanography 7:799-813 doi:10.1029/92PA01267

Bruce J (1974) Some details of upwelling off the Somali and Arabian coasts. Journal of Marine Research 32:419-423

Carr M-E, Kearns EJ (2003) Production regimes in four Eastern Boundary Current systems. Deep Sea Res Part II 50:3199-3221 doi:10.1016/j.dsr2.2003.07.015

Casey KS, Brandon TB, Cornillon P, Evans R (2010) The Past, Present, and Future of the AVHRR Pathfinder SST Program. In: Barale V, Gower JFR, Alberotanza L (eds) Oceanography from Space: Revisited. Springer Netherlands, Dordrecht, pp 273-287. doi:10.1007/978-90-481-8681-5_16

Chavez FP, Bertrand A, Guevara-Carrasco R, Soler P, Csirke J (2008) The northern Humboldt Current System: Brief history, present status and a view towards the future. Prog Oceanogr 79:95-105 doi:10.1016/j.pocean.2008.10.012

Clemens S, Prell W, Murray D, Shimmield G, Weedon G (1991) Forcing mechanisms of the Indian Ocean monsoon. Nature 353:720-725

Currie RI (1992) Circulation and upwelling off the coast of south-east arabia. Oceanol Acta 15:43-60

Curry WB, Ostermann DR, Guptha MVS, Ittekkot V (1992) Foraminiferal production and monsoonal upwelling in the Arabian Sea: evidence from sediment traps. Geol Soc Sp 64:93-106 doi:10.1144/gsl.sp.1992.064.01.06

de Boyer Montégut C, Vialard J, Shenoi SSC, Shankar D, Durand F, Ethé C, Madec G (2007) Simulated Seasonal and Interannual Variability of the Mixed Layer Heat Budget in the Northern Indian Ocean. J Climate 20:3249-3268 doi:10.1175/JCLI4148.1

deCastro M, Sousa MC, Santos F, Dias JM, Gómez-Gesteira M (2016) How will Somali coastal upwelling evolve under future warming scenarios? Scientific Reports 6:30137 doi:10.1038/srep30137

Desbiolles F, Blanke B, Bentamy A, Roy C (2016) Response of the Southern Benguela upwelling system to fine-scale modifications of the coastal wind. Journal of Marine Systems 156:46-55 doi:10.1016/j.jmarsys.2015.12.002

Di Lorenzo E (2015) Climate science: The future of coastal ocean upwelling. Nature 518:310-311 doi:10.1038/518310a

Ekman VW (1905) On the influence of the earth's rotation on ocean currents. Ark Mat Astron Fys 2:1-53

Emeis K-C, Anderson DM, Doose H, Kroon D, Schulz-Bull D (1995) Sea-Surface Temperatures and the History of Monsoon Upwelling in the Northwest Arabian Sea during the Last 500,000 Years. Quaternary Res 43:355-361 doi:10.1006/qres.1995.1041

Feng S, Hu Q (2005) Regulation of Tibetan Plateau heating on variation of Indian summer monsoon in the last two millennia. Geophys Res Lett 32 doi:10.1029/2004GL021246

Findlater J (1969) A major low-level air current near the Indian Ocean during the northern summer. Q J Roy Meteor Soc 95:362-380 doi:10.1002/qj.49709540409

Fischer AS et al. (2002) Mesoscale eddies, coastal upwelling, and the upper-ocean heat budget in the Arabian Sea. Deep Sea Res Part II 49:2231-2264 doi:10.1016/S0967-0645(02)00036-X

Gadgil S (2003) The Indian monsoon and its variability. Annual Review of Earth and Planetary Sciences 31:429-467 doi:10.1146/annurev.earth.31.100901.141251

Giorgetta MA et al. (2013) Climate and carbon cycle changes from 1850 to 2100 in MPI-ESM simulations for the Coupled Model Intercomparison Project phase 5. Journal of Advances in Modeling Earth Systems 5:572-597 doi:10.1002/jame.20038

Godad SP, Naidu PD, Malmgren BA (2011) Sea surface temperature changes during May and August in the western Arabian Sea over the last 22 kyr: Implications as to shifting of the upwelling season. Mar Micropaleontol 78:25-29 doi:10.1016/j.marmicro.2010.09.006

Gutiérrez D et al. (2011) Coastal cooling and increased productivity in the main upwelling zone off Peru since the mid-twentieth century. Geophys Res Lett 38 doi:10.1029/2010GL046324

Halpern D, Feldman GC (1994) Annual and interannual variations of phytoplankton pigment concentration and upwelling along the Pacific equator. J Geophys Res Oceans 99:7347-7354 doi:10.1029/93JC02145

Hurrell JW et al. (2013) The Community Earth System Model: A Framework for Collaborative Research. B Am Meteorol Soc 94:1339-1360 doi:10.1175/BAMS-D-12-00121.1

Huyer A (1983) Coastal upwelling in the California current system. Prog Oceanogr 12:259-284 doi:10.1016/0079-6611(83)90010-1

Ishikawa S, Oda M (2007) Reconstruction of Indian monsoon variability over the past 230,000 years: Planktic foraminiferal evidence from the NW Arabian Sea open-ocean upwelling area. Mar Micropaleontol 63:143-154 doi:10.1016/j.marmicro.2006.11.004

Izumo T, Montégut CB, Luo J-J, Behera SK, Masson S, Yamagata T (2008) The Role of the Western Arabian Sea Upwelling in Indian Monsoon Rainfall Variability. J Climate 21:5603-5623 doi:10.1175/2008JCLI2158.1

Jacox MG, Moore AM, Edwards CA, Fiechter J (2014) Spatially resolved upwelling in the California Current System and its connections to climate variability. Geophys Res Lett 41:3189-3196 doi:10.1002/2014GL059589

Johnson GC, McPhaden MJ, Firing E (2001) Equatorial Pacific Ocean Horizontal Velocity, Divergence, and Upwelling. J Phys Oceanogr 31:839-849 doi:10.1175/1520-0485(2001)031<0839:EPOHVD>2.0.CO;2

Kalnay E et al. (1996) The NCEP/NCAR 40-Year Reanalysis Project. B Am Meteorol Soc 77:437-471 doi:10.1175/1520-0477(1996)077<0437:TNYRP>2.0.CO;2

Keen TR, Kindle JC, Young DK (1997) The interaction of southwest monsoon upwelling, advection and primary production in the northwest Arabian Sea. Journal of Marine Systems 13:61-82 doi:10.1016/S0924-7963(97)00003-1

Kosro PM et al. (1991) The structure of the transition zone between coastal waters and the open ocean off northern California, winter and spring 1987. J Geophys Res Oceans 96:14707-14730 doi:10.1029/91JC01210

Krishnamurthy V, Ajayamohan RS (2010) Composite Structure of Monsoon Low Pressure Systems and Its Relation to Indian Rainfall. J Climate 23:4285-4305 doi:10.1175/2010JCLI2953.1

Kroon D, Steens T, Troelstra SR (1991) Onset Of Monsoonal Related Upwelling In The Western Arabian Sea As Revealed By Planktonic Foraminifers. Proc Ocean Drill Program Sci Results 117:257-263 doi:10.2973/odp.proc.sr.117.126.1991

L'Hégaret P, Duarte R, Carton X, Vic C, Ciani D, Baraille R, Corréard S (2015) Mesoscale variability in the Arabian Sea from HYCOM model results and observations: impact on the Persian Gulf Water path. Ocean Sci 11:667-693 doi:10.5194/os-11-667-2015

Lee CM, Jones BH, Brink KH, Fischer AS (2000) The upper-ocean response to monsoonal forcing in the Arabian Sea: seasonal and spatial variability. Deep Sea Res Part II 47:1177-1226 doi:10.1016/S0967-0645(99)00141-1

Leuschner DC, Sirocko F (2003) Orbital insolation forcing of the Indian Monsoon – a motor for global climate changes? Palaeogeography, Palaeoclimatology, Palaeoecology 197:83-95 doi:10.1016/S0031-0182(03)00387-0

Lévy M, Shankar D, André JM, Shenoi SSC, Durand F, de Boyer Montégut C (2007) Basin-wide seasonal evolution of the Indian Ocean's phytoplankton blooms. J Geophys Res Oceans 112:n/a-n/a doi:10.1029/2007JC004090

Liao X, Zhan H, Wei X (2012) Low-frequency variations in primary production in the Oman upwelling zone associated with monsoon winds. Chinese Journal of Oceanology and Limnology 30:1045-1053 doi:10.1007/s00343-012-1283-8

Lutjeharms JRE, Shillington FA, Rae CMD (1991) Observations of Extreme Upwelling Filaments in the Southeast Atlantic Ocean. Science 253:774-776 doi:10.1126/science.253.5021.774

Ma J, Liu H, Lin P, Zhan H (2014) Seasonality of biological feedbacks on sea surface temperature variations in the Arabian Sea: The role of mixing and upwelling. J Geophys Res Oceans 119:7592-7604 doi:10.1002/2014JC010186

Manghnani V, Morrison JM, Hopkins TS, Böhm E (1998) Advection of upwelled waters in the form of plumes off Oman during the Southwest Monsoon. Deep Sea Res Part II 45:2027-2052 doi:10.1016/S0967-0645(98)00062-9

McGregor HV, Dima M, Fischer HW, Mulitza S (2007) Rapid 20th-Century Increase in Coastal Upwelling off Northwest Africa. Science 315:637-639 doi:10.1126/science.1134839

Murtugudde R, Seager R, Thoppil P (2007) Arabian Sea response to monsoon variations. Paleoceanography 22 doi:10.1029/2007PA001467

Naidu PD, Malmgren BA (1996) A High-resolution record of Late Quaternary upwelling along the Oman Margin, Arabian Sea based on planktonic foraminifera. Paleoceanography 11:129-140 doi:10.1029/95PA03198

Naidu PD, Niitsuma N (2003) Carbon and oxygen isotope time series records of planktonic and benthic foraminifera from the Arabian Sea: implications on upwelling processes. Palaeogeography, Palaeoclimatology, Palaeoecology 202:85-95 doi:10.1016/S0031-0182(03)00629-1

Naik SS, Godad SP, Naidu PD, Ramaswamy V (2013) A comparison of Globigerinoides ruber calcification between upwelling and non-upwelling regions in the Arabian Sea. J Earth Syst Sci 122:1153-1159 doi:10.1007/s12040-013-0330-y

Narayan N, Paul A, Mulitza S, Schulz M (2010) Trends in coastal upwelling intensity during the late 20th century. Ocean Sci 6:815-823 doi:10.5194/os-6-815-2010

Nelson G, Hutchings L (1983) The Benguela upwelling area. Prog Oceanogr 12:333-356 doi:10.1016/0079-6611(83)90013-7

Otto-Bliesner BL et al. (2016) Climate Variability and Change since 850 CE: An Ensemble Approach with the Community Earth System Model. B Am Meteorol Soc 97:735-754 doi:10.1175/BAMS-D-14-00233.1

Pardo PC, Padín XA, Gilcoto M, Farina-Busto L, Pérez FF (2011) Evolution of upwelling systems coupled to the long-term variability in sea surface temperature and Ekman transport. Climate Research 48:231-246

Parthasarathy B, Munot AA, Kothawale DR (1994) All-India monthly and seasonal rainfall series: 1871–1993. Theor Appl Climatol 49:217-224 doi:10.1007/bf00867461

Pauly D, Christensen V (1995) Primary production required to sustain global fisheries. Nature 374:255-257 doi:10.1038/374255a0

Pedlosky J (1978) A Nonlinear Model of the Onset of Upwelling. J Phys Oceanogr 8:178-187 doi:10.1175/1520-0485(1978)008<0178:ANMOTO>2.0.CO;2

Peeters FJC, Brummer G-JA, Ganssen G (2002) The effect of upwelling on the distribution and stable isotope composition of Globigerina bulloides and Globigerinoides ruber (planktic foraminifera) in modern surface waters of the NW Arabian Sea. Global and Planetary Change 34:269-291 doi:10.1016/S0921-8181(02)00120-0

Philander SGH, Yoon J-H (1982) Eastern Boundary Currents and Coastal Upwelling. J Phys Oceanogr 12:862-879 doi:10.1175/1520-0485(1982)012<0862:EBCACU>2.0.CO;2

Pickett MH, Paduan JD (2003) Ekman transport and pumping in the California Current based on the U.S. Navy's high-resolution atmospheric model (COAMPS). J Geophys Res Oceans 108:n/a-n/a doi:10.1029/2003JC001902

Piontkovski SA, Al-Gheilani HM, Jupp BP, Al-Azri AR, Al-Hashmi KA (2012) Interannual changes in the Sea of Oman ecosystem. Open Mar Biol J 6:38-52 doi:10.2174/1874450801206010038

Piontkovski SA, Al-Jufaili S (2013) Coastal upwellings and Mesoscale Eddies of the Western Arabian Sea: Some Biological Implications. Int J Ocean Oceanogr 7:93-115

Prell W, Curry W (1981) Faunal and isotopic indices of monsoonal upwelling-western Arabian Sea. Oceanol Acta 4:91-98

Prell WL, van Campo E (1986) Coherent response of Arabian Sea upwelling and pollen transport to late Quaternary monsoonal winds. Nature 323:526-528 doi:10.1038/323526a0

Price JF, Weller RA, Schudlich RR (1987) Wind-Driven Ocean Currents and Ekman Transport. Science 238:1534-1538 doi:10.1126/science.238.4833.1534

Ranjha R, Tjernström M, Svensson G, Semedo A (2016) Modelling coastal low-level wind-jets: does horizontal resolution matter? Meteorology and Atmospheric Physics 128:263-278 doi:10.1007/s00703-015-0413-1

Rao AD, Joshi M, Ravichandran M (2008) Oceanic upwelling and downwelling processes in waters off the west coast of India. Ocean Dynam 58:213-226 doi:10.1007/s10236-008-0147-4

Rintoul SR, England MH (2002) Ekman Transport Dominates Local Air–Sea Fluxes in Driving Variability of Subantarctic Mode Water. J Phys Oceanogr 32:1308-1321 doi:10.1175/1520-0485(2002)032<1308:ETDLAS>2.0.CO;2

Rixen T, Haake B, Ittekkot V (2000) Sedimentation in the western Arabian Sea the role of coastal and open-ocean upwelling. Deep Sea Res Part II 47:2155-2178 doi:10.1016/S0967-0645(00)00020-5

Robinson MK, Bauer RA (1976) Atlas of North Pacific Ocean Monthly Mean Temperaturs and Mean Salinities of the Surface Layer. Naval Oceanographic Office Reference Publication 2, Washington DC

Rutllant JA, Rosenbluth Bn, Hormazabal S (2004) Intraseasonal variability of wind-forced coastal upwelling off central Chile (30°S). Continental Shelf Research 24:789-804 doi:10.1016/j.csr.2004.02.004

Santos AMP, Kazmin AS, Peliz Á (2005) Decadal changes in the Canary upwelling system as revealed by satellite observations: Their impact on productivity. Journal of Marine Research 63:359-379 doi:10.1357/0022240053693671

Santos F, Gomez-Gesteira M, deCastro M, Alvarez I (2012) Differences in coastal and oceanic SST trends due to the strengthening of coastal upwelling along the Benguela current system. Continental Shelf Research 34:79-86 doi:10.1016/j.csr.2011.12.004

Schott FA (1983) Monsoon response of the Somali Current and associated upwelling. Prog Oceanogr 12:357-381 doi:10.1016/0079-6611(83)90014-9

Schott FA, McCreary Jr JP (2001) The monsoon circulation of the Indian Ocean. Prog Oceanogr 51:1-123 doi:10.1016/S0079-6611(01)00083-0

Schwing FB, Mendelssohn R (1997) Increased coastal upwelling in the California Current System. J Geophys Res Oceans 102:3421-3438 doi:10.1029/96JC03591

Shetye SR, Gouveia AD, Shenoi SSC, Sundar D, Michael GS, Almeida AM, Santanam K (1990) Hydrography and circulation off the west coast of India during the Southwest Monsoon 1987. Journal of Marine Research 48:359-378 doi:10.1357/002224090784988809

Shi W, Morrison JM, Böhm E, Manghnani V (2000) The Oman upwelling zone during 1993, 1994 and 1995. Deep Sea Res Part II 47:1227-1247 doi:10.1016/S0967-0645(99)00142-3

Sinha A, Berkelhammer M, Stott L, Mudelsee M, Cheng H, Biswas J (2011) The leading mode of Indian Summer Monsoon precipitation variability during the last millennium. Geophys Res Lett 38 doi:10.1029/2011GL047713

Sirocko F, Sarnthein M, Lange H, Erlenkeuser H (1991) Atmospheric summer circulation and coastal upwelling in the Arabian Sea during the Holocene and the last glaciation. Quaternary Res 36:72-93 doi:10.1016/0033-5894(91)90018-Z

Small RJ, Curchitser E, Hedstrom K, Kauffman B, Large WG (2015) The Benguela Upwelling System: Quantifying the Sensitivity to Resolution and Coastal Wind Representation in a Global Climate Model. J Climate 28:9409-9432 doi:10.1175/JCLI-D-15-0192.1

Smitha BR, Sanjeevan VN, Vimalkumar KG, Revichandran C (2008) On the Upwelling off the Southern Tip and along the West Coast of India. Journal of Coastal Research:95-102 doi:10.2112/06-0779.1

Sydeman WJ, García-Reyes M, Schoeman DS, Rykaczewski RR, Thompson SA, Black BA, Bograd SJ (2014) Climate change and wind intensification in coastal upwelling ecosystems. Science 345:77-80 doi:10.1126/science.1251635

Thadathil P et al. (2008) Seasonal Variability of the Observed Barrier Layer in the Arabian Sea. J Phys Oceanogr 38:624-638 doi:10.1175/2007JPO3798.1

Tim N, Zorita E, Hünicke B (2015) Decadal variability and trends of the Benguela upwelling system as simulated in a high-resolution ocean simulation. Ocean Sci 11:483-502 doi:10.5194/os-11-483-2015

Tim N, Zorita E, Hünicke B, Yi X, Emeis KC (2016) The importance of external climate forcing for the variability and trends of coastal upwelling in past and future climate. Ocean Sci 12:807-823 doi:10.5194/os-12-807-2016

Tozuka T, Nagura M, Yamagata T (2014) Influence of the Reflected Rossby Waves on the Western Arabian Sea Upwelling Region. J Phys Oceanogr 44:1424-1438 doi:10.1175/JPO-D-13-0127.1

Traganza ED, Conrad JC, Breaker LC (1981) Satellite Observations of a Cyclonic Upwelling System and: Giant Plume in the California Current. In: Coastal Upwelling. American Geophysical Union, pp 228-241. doi:10.1029/CO001p0228

Tudhope AW, Lea DW, Shimmield GB, Chilcott CP, Head S (1996) Monsoon climate and Arabian Sea coastal upwelling recorded in massive corals from southern Oman. PALAIOS 11:347-361 doi:10.2307/3515245

Turner AG, Joshi M, Robertson ES, Woolnough SJ (2012) The effect of Arabian Sea optical properties on SST biases and the South Asian summer monsoon in a coupled GCM. Climate Dynamics 39:811-826 doi:10.1007/s00382-011-1254-3

Varela R, Álvarez I, Santos F, deCastro M, Gómez-Gesteira M (2015) Has upwelling strengthened along worldwide coasts over 1982-2010? Scientific Reports 5:10016 doi:10.1038/srep10016

von Bodungen B, John HC, Lutjeharms JRE, Mohrholz V, Veitch J (2008) Hydrographic and biological patterns across the Angola–Benguela Frontal Zone under undisturbed conditions. Journal of Marine Systems 74:189-215 doi:10.1016/j.jmarsys.2007.12.007

von Storch H, Zwiers FW (2001) Statistical Analysis in Climate Research. Cambridge University Press, Cambridge, UK

von Storch J-S et al. (2012) An Estimate of the Lorenz Energy Cycle for the World Ocean Based on the STORM/NCEP Simulation. J Phys Oceanogr 42:2185-2205 doi:10.1175/JPO-D-12-079.1

Wang B, Fan Z (1999) Choice of South Asian Summer Monsoon Indices. B Am Meteorol Soc 80:629-638 doi:10.1175/1520-0477(1999)080<0629:COSASM>2.0.CO;2

Wang D, Gouhier TC, Menge BA, Ganguly AR (2015) Intensification and spatial homogenization of coastal upwelling under climate change. Nature 518:390-394 doi:10.1038/nature14235

Webster PJ, Yang S (1992) Monsoon and Enso: Selectively Interactive Systems. Q J Roy Meteor Soc 118:877-926 doi:10.1002/qj.49711850705

Weller RA, Baumgartner MF, Josey SA, Fischer AS, Kindle JC (1998) Atmospheric forcing in the Arabian Sea during 1994–1995: observations and comparisons with climatology and models. Deep Sea Res Part II 45:1961-1999 doi:10.1016/S0967-0645(98)00060-5

Weller RA et al. (2002) Moored observations of upper-ocean response to the monsoons in the Arabian Sea during 1994–1995. Deep Sea Res Part II 49:2195-2230 doi:10.1016/S0967-0645(02)00035-8

Wiggert JD, Murtugudde RG, McClain CR (2002) Processes controlling interannual variations in wintertime (Northeast Monsoon) primary productivity in the central Arabian Sea. Deep Sea Res Part II 49:2319-2343 doi:10.1016/S0967-0645(02)00039-5

Wooster WS, Bakun A, McLain DR (1976) Seasonal upwelling cycle along the eastern boundary of the North Atlantic. Journal of Marine Research 34:131-141

Wyrtki K (1981) An Estimate of Equatorial Upwelling in the Pacific. J Phys Oceanogr 11:1205-1214 doi:10.1175/1520-0485(1981)011<1205:AEOEUI>2.0.CO;2

Yelland M, Taylor PK (1996) Wind Stress Measurements from the Open Ocean. J Phys Oceanogr 26:541-558 doi:10.1175/1520-0485(1996)026<0541:WSMFTO>2.0.CO;2

List of Figures

List of Tables

List of Publications

Yi X, Hünicke B, Tim N, Zorita E (2016) The relationship between Arabian Sea upwelling and Indian Monsoon revisited in a high resolution ocean simulation. (Revision submitted)

Yi X, Hünicke B, Zorita E (2016) Arabian Sea upwelling over the last millennium and in the 21st century as simulated by Earth System Models. (In preparation)

Tim N, Zorita E, Hünicke B, Yi X, Emeis KC (2016) The importance of external climate forcing for the variability and trends of coastal upwelling in past and future climate Ocean Sci 12:807-823 doi:10.5194/os-12-807-2016

Acknowledgement

I would like to express my deepest gratitude to my thesis supervisor Dr. Eduardo Zorita, not only for his guidance during my PhD work, but also for his help on my life here in Germany. Whenever I encounter problems, he is always there with his door open, smiling. His knowledge and patience have deeply encouraged me. I would also like to thank Dr. Birgit Hünicke for being my "Doktormutter". She has helped me in many ways and I could not have finished my work at this time without her support.

My sincere appreciation goes to Prof. Dr. Kay-Christian Emeis. As my panel chair, Prof. Emeis has helped me with many useful suggestions related to my work. It is always an enjoyable and inspirable time to read his comments on my panel meeting reports.

I am very grateful to Dr. Nele Tim and Dr. Svenja Bierstedt. It is always relaxing to talk with them, no matter if it is for work or life. I appreciate their help through my entire PhD work, and especially for translating my thesis abstract to "Zusammenfassung".

This work is part of the project of Universität Hamburg's Cluster of Excellence "Integrated Climate System Analysis and Prediction" (CliSAP) funded by the German Research Foundation (DFG). I would like to thank School of Integrated Climate System Sciences (SICSS) for accepting me as a member and Helmholtz-Zentrum Geesthacht for providing the position.

Special thanks go to my family and friends for always supporting and encouraging me. Most of all, the biggest thank you goes to my girlfriend Xin Liu for her understanding, her tolerance, and her love. She is my lighthouse so no matter what happens at work I always know my way back home.

Eidesstattliche Versicherung

Declaration on oath

Hiermit erkläre ich an Eides statt, dass ich die vorliegende Dissertationsschrift selbst verfasst und keine anderen als die angegebenen Quellen und Hilfsmittel benutzt habe.

I hereby declare, on oath, that I have written the present dissertation on my own and have not used other than the acknowledged resources and aids.

Hamburg 2016